Improved Biomass Estimation Using the Texture Parameters of Two High-Resolution Optical Sensors

Janet E. Nichol and Md. Latifur Rahman Sarker

***Abstract*—Accurate forest biomass estimation is essential for greenhouse gas inventories, terrestrial carbon accounting, and climate change modeling studies. Unfortunately, no universal and transferable technique has been developed so far to quantify biomass carbon sources and sinks over large areas because of the environmental, topographic, and biophysical complexity of forest ecosystems. Among the remote sensing techniques tested, the use of multisensors and the spatial as well as the spectral characteristics of the data have demonstrated a strong potential for forest biomass estimation. However, the use of multisensor data accompanied by spatial data processing has not been fully investigated because of the unavailability of appropriate data sets and the complexity of image processing techniques in combining multisensor data with the analysis of the spatial characteristics. This paper investigates the texture parameters of two high-resolution (10 m) optical sensors (Advanced Visible and Near Infrared Radiometer type 2 (AVNIR-2) and SPOT-5) in different processing combinations for biomass estimation. Multiple regression models are developed between image parameters extracted from the different stages of image processing and the biomass of 50 field plots, which was estimated using a newly developed "allometric model" for the study region. The results demonstrate a clear improvement in biomass estimation using the texture parameters of a single sensor ($r^2 = 0.854$ and rmse $= 38.54$) compared to the best result obtained from simple spectral reflectance ($r^2 = 0.494$) and simple spectral band ratios ($r^2 = 0.59$). This was further improved to obtain a very promising result using the texture parameter of both sensors together ($r^2 = 0.897$ and rmse $= 32.38$), the texture parameters from the principal component analysis of both sensors ($r^2 = 0.851$ and rmse $= 38.80$), and the texture parameters from the averaging of both sensors ($r^2 = 0.911$ and rmse $= 30.10$). Improvement was also observed using the simple ratio of the texture parameters of AVNIR-2 ($r^2 = 0.899$ and rmse $= 32.04$) and SPOT-5 ($r^2 = 0.916$), and finally, the most promising result ($r^2 = 0.939$ and rmse $= 24.77$) was achieved using the ratios of the texture parameters of both sensors together. This high level of agreement between the field and image data derived from the two novel techniques (i.e., combination/fusion of the multisensor data and the ratio of the texture parameters) is a very significant improvement over previous work where agreement not exceeding $r^2 = 0.65$ has been achieved using optical sensors. Furthermore, biomass estimates of up to 500 t/ha in our study area far exceed the saturation levels observed in other studies using optical sensors.**

***Index Terms*—Biomass estimation, multisensors, texture measurement.**

I. Introduction

THE RECENT United Nations Climate Conference in Copenhagen, Denmark, in December 2009 once again reminded us that climate change is one of the most severe problems on Earth and that the atmospheric content of greenhouse gas (particularly CO_2), which has risen precipitously in the last 250 years, particularly in the last 50 years [1], is the main culprit. Forests can remove this CO_2 from the atmosphere in the process of photosynthesis and can store it in their biomass, thereby lessening the greenhouse effect [2]. Thus, forest biomass is considered as an important part of the global carbon cycle [3]–[5]. As a result, accurate forest biomass estimation is required for many purposes including greenhouse gas inventories, terrestrial carbon accounting, climate change modeling [6]–[11], and implementation of the Kyoto Protocol of the United Nations Framework Convention on Climate Change. Unfortunately, this estimation is not straightforward, and no universal and transferable technique for quantifying carbon sources and sinks has been developed so far [12], [13] because of the environmental, topographic, and biophysical complexity of forest ecosystems, which differ in time and space. Besides traditional field-based methods, which are accurate but costly, time consuming, and limited to small areas [14]–[19], remote sensing is the most promising technique for estimating biomass at local, regional, and global scales [20]–[26]. A number of studies has been carried out using different types of sensors, including optical [4], [5], [26]–[41], synthetic aperture radar (SAR) [42]–[53], and lidar sensors [54]–[58], for biomass/forest parameter estimation.

Apart from the use of a single sensor, combining information from multiple sensors has yielded promising results for the estimation of forest parameters/biomass [13], [18], [19], [59]–[62]. A useful approach is to combine SAR and optical sensors [60], [61], [63], [64], but many other options have been tested, including different frequencies and polarizations [21], [65]–[72], different sensors [10], [18], [19], [64], [73]–[78], and multiple spatial resolutions [79], and improvements have been obtained because different sensors often have complementary characteristics in their interaction with land surfaces [61], [60]. From this broad range of approaches, widely varying degrees of success have been obtained because of the complexity of

Manuscript received January 22, 2010; revised June 1, 2010; accepted July 5, 2010. Date of publication October 14, 2010; date of current version February 25, 2011. This work was supported by GRF Grant PolyU5281/09E.

J. E. Nichol is with the Department of Land Surveying and Geo-Informatics, The Hong Kong Polytechnic University, Kowloon, Hong Kong (e-mail: lsjanet@inet.polyu.edu.hk).

M. L. R. Sarker is with the Department of Land Surveying and Geo-Informatics, The Hong Kong Polytechnic University, Kowloon, Hong Kong, and also with the Rajshahi University, Rajshahi 6205, Bangladesh (e-mail: lrsarker@yahoo.com).

Color versions of one or more of the figures in this paper are available online at http://ieeexplore.ieee.org.

Digital Object Identifier 10.1109/TGRS.2010.2068574

biomass in time and space, the lack of comprehensive field data, and the limitations in the spatial and spectral characteristics of the satellite data.

Beyond the shortcomings of the data, processing techniques may be the most important factor in biomass estimation as previous research has shown that the simple reflectance of the optical sensors [25], [26], [28], [31], [36], [80]–[82] and the backscattering of the radar sensors [46], [68], [70], [72], [83], [84] are unable to provide good estimations. Thus, processing techniques need to be selected to complement suitable data configurations.

Now that optical sensors with a wide range of spatial and spectral resolutions are available, optical sensors are still an attractive data source, even though previous research has shown the difficulty of biomass estimation based on raw spectral signatures because of the influence of increased canopy shadowing within large stands, the heterogeneity of vegetation stand structures, and the spectral data saturation [5], [25], [26], [30], [31], [38], [85]–[89]. However, vegetation indices, which have the ability to minimize contributions from the soil background, sun angle, sensor view angle, senesced vegetation, and the atmosphere [90]–[95], are proven to be more successful [25], [31], [37], [38], [85], [89], [96]–[98] but still with generally low to moderate accuracies of up to ca. 65%. Moreover, these moderate results have been obtained in temperate forests because of their simple canopy structure and tree species composition. In tropical and subtropical regions where biomass levels are high, where the forest canopy is closed with multiple layering, and where a great diversity of species is present ([21], [25], [26], [31], [38], [85], [86], vegetation indices have shown less potential, with low or insignificant results.

On the other hand, the spatial characteristics of images, such as texture, have been able to identify objects or regions of interest in an image [99], and image texture is particularly useful in fine spatial resolution imagery [61]. Many of the texture measures developed [99], [100]–[102] have shown potential for improvements in land use/land cover mapping using both optical and SAR images [103]–[114]. Image texture has also proved to be capable of identifying different aspects of forest stand structure, including age, density, and leaf area index ([53], [115]–[119]) and has shown a potential for biomass estimation with both optical [5], [38], [89] and SAR data ([42], [51], [120]. Moreover, although most previous biomass estimation projects used Landsat TM data with a 30-m spatial resolution [60], texture is expected to be more effective with finer spatial resolution imagery since finer structural details can be distinguished [51], [61], [110], [121]–[125]. Two potential drawbacks of the implementation of texture measurement for biomass estimation are the following: 1) texture is a very complex property and can vary widely depending on the object of interest, the environmental conditions, and the selection of window size [105], [119], [126], [127], and 2) texture processing can generate a lot of data which are difficult to manage [119], [127]. Thus, although texture measurement holds potential for biomass estimation, it has not yet been fully investigated, and results so far, when applying texture to optical images, have not exceeded 65% accuracy, even in structurally simple temperate and boreal forests [5].

Considering the potential advantages of both image texture and multisensor data, this paper investigates texture processing for biomass estimation using data from two high-resolution optical sensors ANVIR-2 and SPOT-5 along with raw spectral processing and some simple band ratios. The project data were selected by considering the following facts: 1) both sensors have fine spatial resolution (10 m), and this higher spatial resolution shows promise for image texture analysis; 2) the sensors have some common spectral bands (green, red, and NIR) which may help in reducing any random error in the averaging process; and 3) the sensors have uncommon spectral bands (blue in Advanced Visible and Near Infrared Radiometer type 2 (AVNIR-2) and short-wave near infrared (SWNIR) in SPOT-5) which may be able to provide complementary information.

A. Objectives

The overall objective of the study is to explore the potential of texture processing combined with multisensor capability for the improvement of biomass estimation using data from two high-resolution optical sensors. More specific objectives are to investigate the performance of the following:

1) the spectral reflectance of the individual bands of the sensors individually and together;
2) the simple ratio of the different bands of the sensors individually and jointly;
3) the texture parameters of the sensors individually and together;
4) the simple ratio of the texture parameters of the sensors individually and together for the improvement of biomass estimation.

II. Study Area and Data

A. Study Area

The study area for this research is the Hong Kong Special Administrative Region (Fig. 1) which lies on the southeast coast of China, just south of the Tropic of Cancer. The total land area of Hong Kong is 1100 km^2, which includes 235 small outlying islands. Although the population is over 7 million, only about 15% of the territory is built-up, but less than 1% is still actively cultivated. Approximately 40% of the total area is designated as country parks, which are reserved for forest succession under the management of the Agriculture, Fisheries and Conservation Department. The native subtropical evergreen broad leaf forest has been replaced by a complex patchwork of regenerating secondary forest in various stages of development, and plantations. Forest grades into woodland, shrubland, and then grassland at higher elevations.

B. Data

Images from two optical sensors were used in this paper. One image was obtained on October 24, 2007, by AVNIR-2 from the ALOS-2 satellite launched in January 2006, and the other was collected on December 31, 2006, by the High-Resolution

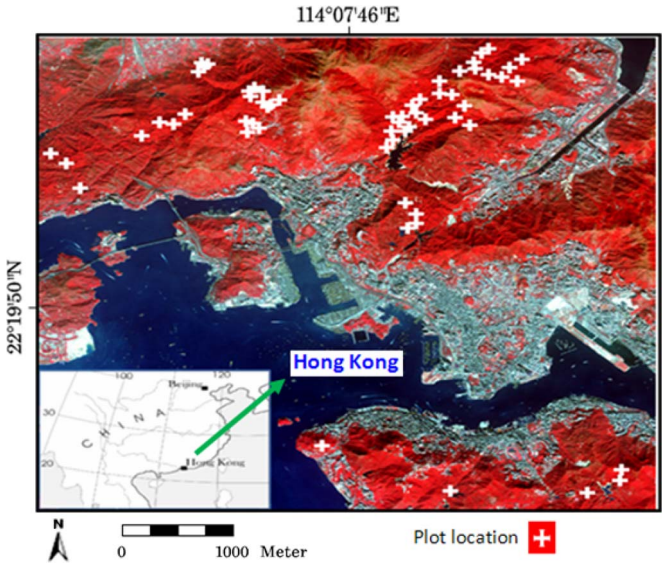

Fig. 1. Study area and sample plots.

Geometric (HRG) sensor of the SPOT-5 Earth Observation Satellite launched in May 2002 (Table I). The instantaneous field of view of 10 m for the AVNIR-2 multispectral sensor is the main improvement over the 16-m resolution AVNIR. The SPOT-5 HRG multispectral data add an improved spatial resolution (20 to 10 m) compared with the previous SPOT-4 platform as well as an additional shortwave infrared band at 10 m. With swath widths of 70 and 60 km, respectively, both AVNIR-2 and SPOT-5 HRG are suitable for regional scale monitoring and ideal for Hong Kong's land area of ca. 40 × 60 km.

III. Methodology

The methodology (Fig. 2) of this paper comprises two parts, namely, allometric model development for field biomass estimation and processing of AVNIR-2 and SPOT-5 images.

A. Allometric Model Development

Due to the lack of an allometric model for converting the trees measured in the field to actual biomass, it was necessary to harvest, dry, and measure a representative sample of trees. Since Hong Kong's forests are very diverse, the harvesting of a large sample was required. This was done by selecting the dominant tree species comprising a total of 75 trees in 4 diameter at breast height (DBH) classes (less than 10, 10–15, 15–20, and 20 cm and above), and standard procedures were followed for tree harvesting [14], [128], [129].

The harvested trees were separated into fractions, including leaves, twigs, small branches, large branches, and stem. After measuring the fresh weight (FW), representative samples (Fig. 3) from every part of the tree were taken for dry weight (DW) measurement in an oven at 80 °C until a constant DW was obtained (Fig. 3). The weight of every sample was estimated using the same electric weight balance at a 0.002-g precision. The ratio of DW to FW was calculated for every part of the samples using DW and FW of each part of the tree. Using the ratio, DW was calculated for every part, and finally, the DW of each tree was calculated by summing the DW of all parts.

Regression models used by previous researchers [20], [128] were tested in order to find the best fit by using DW as the dependent variable and DBH and height as independent variables in different combinations. Finally, using the log transformed DBH and DW, the best fit model (Table II) was found, considering all test parameters including the correlation coefficient (r), the coefficient of determination (r^2), the adjusted coefficient of determination (adjusted r^2), and the rmse. A fit of approximately 93.2% (adjusted r^2 of 0.932) and an rmse of 13.50 were obtained for this best fit model (Table II). This was deemed highly satisfactory in view of the great variety of tree species, and is similar to the accuracies of several other specialist forest inventories [20], [128].

B. Field Plot Measurement and Field Biomass Estimation

To build a relationship between image parameters and field biomass, 50 sample plots covering a variety of tree stand types were selected using purposive sampling. Circular plots with a 15-m radius were determined by considering the image resolution (approximately 10 m), the orthorectification error, and the GPS positioning error. All sample plots were positioned within a homogenous area of the forest and at least 15 m distant from other features such as roads, water bodies, and other infrastructure. A Leica GS5+ GPS was used to determine the center of each plot using the Differential Global Positioning System mode for accuracy within ±3 m. For a precise position, a Position Dilution of Precision value below four was always attempted. Both DBH and tree height were measured for all trees within the circular plot region. The DBH of the trees was measured at 1.3 m above the ground, and the heights of the small and large trees were measured by Telescopic-5 and DIST pro4, respectively. Trees with a DBH below 2.5 cm were not included but were recorded. Finally, using the measured parameter DBH, the biomass of each tree and the biomass of all trees in a plot were estimated (Table III) using the allometric model developed for this study area.

C. AVNIR-2 and SPOT-5 Data Preprocessing

The digital number values of the AVNIR-2 and SPOT-5 data were converted to spectral radiance using the conversion factors given in the image header files. Orthorectification was carried out using the Satellite Orbital Math Model to compensate distortions such as sensor geometry, satellite orbit and attitude variations, Earth shape, rotation, and relief. In order to ensure an rms error within 0.5 pixel, a high-resolution (10 m) digital elevation model and well-distributed ground control points were used for orthorectification.

D. Texture Analysis

Texture is a function of local variance in the image, which is related to the spatial resolution and size of the dominant scene objects [130], and it can be used to identify these objects or

TABLE I
CHARACTERISTICS OF THE DATA USED FOR THIS PAPER

	AVNIR-2	SPOT-5
Band and Wavelengths	Band 1: (blue), 0.42 to 0.50 Band 2: (green), 0.52 to 0.60 Band 3: (red), 0.61 to 0.69 Band 4: (near-IR), 0.76 to 0.89	Band 1: (green), 0.50-0.59 Band 2: (red), 0.61-0.68 Band 3: (near-IR), 0.78-0.89 Band 4: (Shortwave IR), 1.580-1.750
Spatial Resolution (m)	10m	10m
Bit Length	8	8
Swath width	70km (at Nadir)	60 Km x 60 Km to 80 Km at nadir
Orbital Altitude	Approximately 692km	822 kilometers
Orbital Inclination	98.2°, Sun Synchronous	98.7°, Sun-synchronous
Revisiting Time	Sub cycle: 2 days	2-3 days, depending on latitude

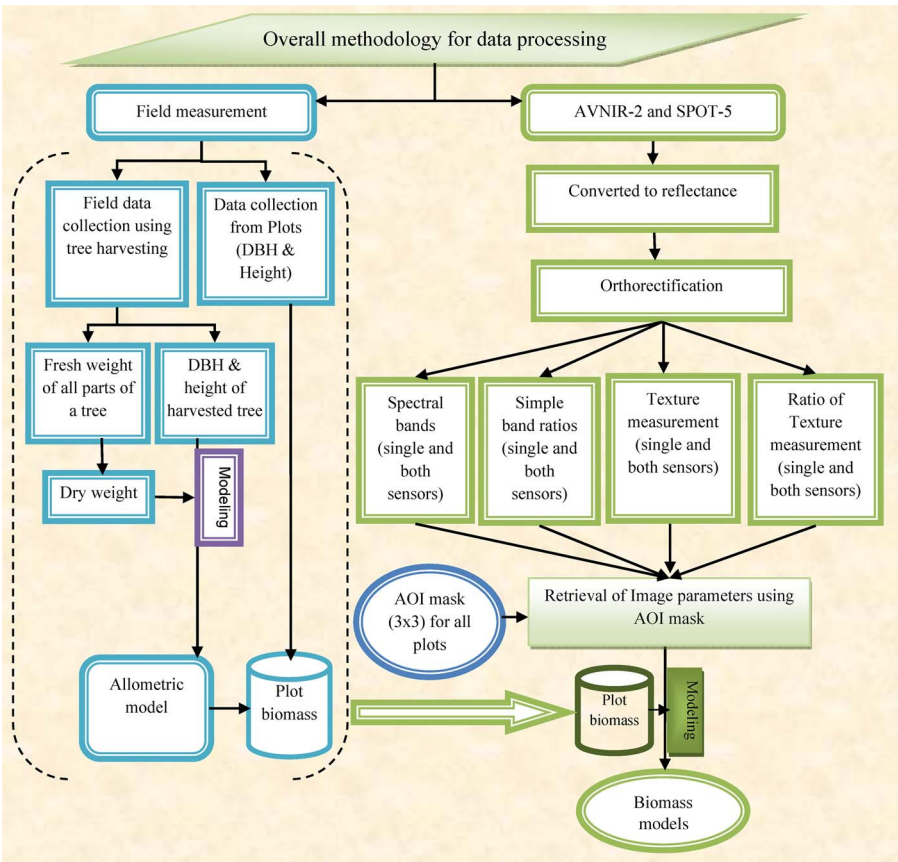

Fig. 2. Overall methodology.

regions of interest in any image [99], [131]. Studies have shown that, in many cases, texture may be a more important source of information than reflectance or intensity, and this is especially true in high-resolution images (e.g., [61], [69], [112], [132], and [133]). Thus, in forested landscapes, texture is dependent on the size and spacing of tree crowns, and on high-resolution images if a pixel falls on a tree, its neighbor may also fall on the same tree, resulting in a low local variance. As the resolution increases to a level that is comparable to the dominant tree crown size, the local variance increases, and this should be especially true in tropical forests with high species diversity, where stands are heterogeneous [130].

Several methods and techniques for describing texture, based on statistical models, have been developed [51], [112], [113], [120]. For this paper, two categories of texture measurement were selected to test their potential for biomass estimation with AVNIR-2 and SPOT-5 data (Table IV). The first one is the gray level co-occurrence matrix (GLCM) [99] along with some gray level difference vector based texture measurements. The second one is the sum and difference histogram proposed by the

Fig. 3. Tree harvesting procedure for the allometric model development.

authors in [134] as an alternative to the usual co-occurrence matrices used. Identifying suitable textures additionally involves the selection of moving window sizes [38], [127]. A small window size exaggerates the difference within the window (local variance) but retains a high spatial resolution, while a large window may not extract the texture information efficiently due to over-smoothing of the textural variations. Because the resolution of the data used is high (approximately 10 m) and the forest structure in the study area is dense and compact, all texture measurements were performed using four small to medium window sizes from 3×3 to 9×9.

E. Statistical Analysis

To represent the relationship between field biomass and remotely sensed data, some researchers have used linear regression models with or without log transformation of the field biomass data [28], [31], [34], [35], [65], [66], [83], while others have used multiple regression with or without stepwise selection [18], [19], [26], [27], [37], [46], [69]–[71], [98]. Nonlinear regression [45], [135], artificial neural networks [4], [25], [26], [136]–[138], semiempirical models [48], and nonparametric estimation methods such as k-nearest neighbor and k-means clustering have also been widely used [139]. Although no model can perfectly express this complex relationship, researchers are still using multiple regression models as one of the best choices. In this paper, simple linear regression and stepwise multiple-linear regression models were used to compare the data derived from all processing steps with field biomass. The biomass data were collected from 50 field plots and were used as independent variables. The spectral reflectance of each field plot was extracted using an area-of-interest mask of 3×3 pixels, for which the mean reflectance was calculated.

In multiple regression modeling, difficulties such as multicollinearity and overfitting may arise when a large number of independent variables are used, such that the independent variables are highly correlated with one another. To avoid overfitting problems as well as to ensure finding the best fit model, five common statistical parameters, namely, the correlation coefficient (r), the coefficient of determination (r^2), the adjusted r^2, the rmse, and the p-level (for the model), were computed. Another seven statistical parameters such as the beta coefficient (B), the standard error of B, the p-level, the tolerance $(\text{Tol} = \text{Tolerance} = 1 - R_x^2)$, the variance inflation factor $(\text{VIF}_j = 1/1 - R_j^2)$, the eigen value (EV), and the condition index $(\text{CI} = k_j = (\lambda_{\max}/\lambda_j),\ j = 1, 2, \ldots, p)$ were calculated to test the intercept fitness and multicollinearity effects. To indicate multicollinearity problems, a tolerance value that is less than 0.10 [140], a VIF value that is greater than 10 [19], [140]–[142], an EV that is close to zero [142], [143], and a condition index that is greater than 30 [140], [142], [143] were used as determinants.

F. Processing of the AVNIR-2 and SPOT-5 Data for Modeling

The data of AVNIR-2 and SPOT-5 were processed in the following three steps.

First Processing Step—Spectral Bands and Simple Band Ratio: To test the potential of the spectral reflectance of all bands of one sensor and both sensors together and the ratios, the following bands and simple band ratios were used in the model.

1) The spectral reflectance extracted from all four bands of ANVIR-2 and SPOT-5 were used individually in a linear regression model, and all bands of a single sensor were used in a multiple regression model.
2) The spectral reflectance extracted from all bands of ANVIR-2 and SPOT-5 and the principal component analysis (PCA) of all bands of both sensors were used together using a stepwise multiple regression model.
3) The spectral reflectance extracted from all six simple spectral band ratios (1/2, 1/3, 1/4, 2/3, 2/4, and 3/4) of both sensors was used individually in a simple regression model. Multiple regression models were also used to test all simple band ratios of each sensor together.
4) The spectral reflectance extracted from all simple band ratios (1/2, 1/3, 1/4, 2/3, 2/4, and 3/4) of both sensors was used together in stepwise multiple regression models.

Second Processing Step—Modeling of the Texture Parameters: Fifteen types of texture measurements using four window sizes (from 3×3 to 9×9) were used to generate the texture parameters from four spectral bands (each of the AVNIR-2 and SPOT-5 data). All texture-derived parameters were used in the model in the following manner.

1) The texture parameters derived from each band of both sensors and all texture parameters of a single sensor were used in the stepwise multiple regression model.
2) The texture parameters derived from both sensors together were used in the multiple regression model.
3) The texture parameters derived from the PCA of both sensors were used in the multiple regression model.
4) The texture parameters derived from the band averaging of both sensors were used in the multiple regression model.

Third Processing Step—Modeling the Simple Ratio of the Texture Parameters: In this processing step, six types of ratios (1/2, 1/3, 1/4, 2/3, 2/4, and 3/4) were performed using the

TABLE II
BEST FIT ALLOMETRIC MODEL

Regression Model	Coefficient & Value		Std Err. of Coef.	Multiple R	R^2	Adjusted R^2	RMSE	p
InDW = a + b * In DBH	a	-2.057	.183	.966	.933	932	13.525	.0005
	b	2.289	.072					

TABLE III
DW (BIOMASS) DISTRIBUTION OF SELECTED FIELD PLOTS

Biomass range (t/ha)	Biomass of each plots	Number of plots	Percentage of plots
50-100	50.52, 57.45, 57.53, 61.14, 77.46, 78.11, 82.38, 83.24, 83.87, 92.16, 93.46, 94.68	12	24
100-150	104.60, 106.56, 107.04, 108.10, 109.39, 110.98, 111.67, 120.36, 122.96, 124.13, 131.55, 132.64, 133.07, 136.20, 138.04, 141.90, 147.49, 149.64	18	36
150-200	150.18, 151.46, 156.69, 157.44, 157.59, 163.14, 166.56, 168.02, 177.49, 178.49, 178.89, 188.62, 189.35	13	26
200 & above	270.87, 312.05, 317.93, 346.09, 360.84, 518.60, 530.00	7	14
Total		50	100

texture parameters of both sensors, and modeling was performed in the following ways.

1) The parameters derived from each texture parameter ratio were used in the multiple regression model.
2) The parameters derived from all six simple texture band ratios of an individual sensor were used in the multiple regression model.
3) The parameters derived from all texture parameter ratios of both sensors were used in the stepwise multiple regression model together.

IV. RESULTS AND ANALYSIS

The field data collected from 50 field plots showed a wide range of biomass levels from 52 to 530 t/ha. The average of ca. 150 t/ha biomass for our secondary forest study area is more than twice the biomass levels for other reported tropical secondary forests [86] and is representative of a wide variety of successional stages and tree sizes in the study area. For example, most forest is younger than 70 years old, with a biomass below 200 t/ha. The fewer plots above this level reflect the more restricted distribution of late successional stage forest. In all modeling processes, the 50 field plots were used as the dependent variable, and the parameters derived from different processing steps (AVNIR-2 and/or SPOT-5) were used as independent variables. The results of the three processing steps are presented as three separate sections.

A. Performance of the Raw Bands and Simple Band Ratio

The best estimates of biomass using simple spectral bands from AVNIR-2 and SPOT-5, as well as different combinations of bands and PCA, produced only ca. 50% usable accuracy. From the individual bands of both sensors, best result ($r^2 = 0.494$ for AVNIR-2 and $r^2 = 0.316$ for SPOT-5) was obtained from the NIR bands, and the lowest performance ($r^2 = 0.002$ for AVNIR-2 and $r^2 = 0.0345$ for SPOT-5) was obtained from the red bands [Fig. 4(a) and (b)]. The performance of the model (r^2) increased to 0.631 and 0.503 using all bands of AVNIR-2 and SPOT-5, respectively. Combining all bands of both sensors together was not able to produce a better performance because of a strong intercorrelation among bands. However, although multiband models appear to improve biomass estimation accuracy, the problem is that these models violate the assumption of uncorrelated independent variables and show strong multicollinearity effects (a CI that is more than 30) except for the PCA-based model which was only able to define field biomass with an accuracy of approximately 50%.

The simple band ratios of both sensors (individually and together) improved biomass estimation substantially [Fig. 5(a) and (b)], with the highest r^2 of 0.59 being derived from the red/NIR ratio of AVNIR-2, compared to the highest performance for SPOT-5 of $r^2 = 0.387$ also from the red/NIR ratio. This improvement may be explained by the fact that ratios can enhance the vegetation signal while minimizing the solar irradiance, soil background, and topographic effects [90], [92], [93], [119], [144]–[152]. In addition to the assessment of single band ratios, multiple regression models were developed using all simple band ratios of AVNIR-2 and SPOT-5 for each sensor individually and both together. The results [Fig. 5(c)] showed a significant improvement in biomass estimation, with an r^2 of 0.739 obtained from the combined use of simple ratios of both

TABLE IV
FORMULAS OF THE TEXTURE MEASUREMENTS USED IN THIS PAPER

Gray level co-occurrence matrix (GLCM) based texture parameter estimation	Sum and difference histogram (SADH) based texture parameter
1. $Mean(ME) = \sum_{i,j=0}^{N-1} i\ P_{i,j}$ 2. $Homogeneity(HO) = \sum_{i,j=0}^{N-1} i \frac{P_{ij}}{1+(i-j)^2}$ 3. $Contrast(CO) = \sum_{i,j=0}^{N-1} i\ P_{i,j}\ (i-j)^2$ 4. $Standard\ deviation(Std) = \sqrt{VA}$ $where\ VA == \sum_{i,j=0}^{N-1} i\ P_{i,j}\ (i-ME)^2$ 5. $Dissimilarity(DI) = \sum_{i,j=0}^{N-1} i\ P_{i,j}\ \lvert i-j \rvert$ 6. $Entropy(EN) = \sum_{i,j=0}^{N-1} i\ P_{i,j}\ \left(-\ln P_{i,j}\right)$ 7. $Angula\ Second\ Moment\ (ASM) = \sum_{i,j=0}^{N-1} i\ P_{i,j}^2$ 8. $Correlation(CR) = \sum_{i,j=0}^{N-1} i\ P_{i,j} \left[\frac{(i-ME)(j-ME)}{\sqrt{VA_i\ VA_j}}\right]$ 9. $Inverse\ Difference(ID) = \sum_{i,j=0}^{N-1} i \frac{P_{ij}}{\lvert i-j \rvert^2}$ 10. $GLDV\ Angular\ Second\ Moment\ (GASM) = \sum_{k=0}^{N-1} V_k^2$ 11. $GLDV\ Entropy\ (GEN) = \sum_{k=0}^{N-1} V_k\ (-\ln V_k)$ 12. $GLDV\ Mean\ (GME) = \sum_{k=0}^{N-1} k\ V_k$ 13. $GLDV\ Contrast\ (GCO) = \sum_{k=0}^{N-1} k^2\ V_k$ Here, P (i, j) is the normalized co-occurrence matrix such that SUM (i , j=0, N-1) (P (i, j)) = 1. V(k) is the normalized grey level difference vector V(k) = SUM (i, j=0, N-1 and |i-j | = k) P (i, j)	1. $Mean\ (\mu) = \frac{\sum_{i,j} x_{ij}}{n}$ $\sum_{i,j} \frac{[\square \lvert x_{ij} - \mu \rvert \square]}{n}$ 3. $Mean\ Euclidean\ distance\ (MED) = \sqrt{\frac{\sum_{i,j} \left(x_{ij} - x_c\right)^2}{n-1}}$ 4. $Variance\ (\sigma^2) = \frac{\sum_{i,j} \left(x_{ij} - \mu\right)^2}{n-1}$ 5. $Normalized\ Coefficient\ of\ Variation(NCV) = \sqrt{\frac{\sigma^2}{\mu}}$ 6. $Skewness\ (Sk) = \frac{\sum_{i,j} \left(x_{ij} - \mu\right)^3}{(n-1)\sigma^3}$ 7. $Kurtosis\ (Ku) = \frac{\sum_{i,j} \left(x_{ij} - \mu\right)^4}{(n-1)\sigma^4}$ 8. $Energy(E) = \sum_{i,j} x_{ij}^2$ 9. $Entropy\ (H) = -\sum_{i,j} p_{ij} \ln\left([p_{ij}\right), \quad with\ p_{ij} = \frac{x_{ij}}{\sum_{i,j} x_{ij}}$ Here, x_{ij} stands for the pixel value of pixel (i, j) in the kernel over which is summed, n for the number of pixels that is summed, x_c for the kernel's center pixel value, and p_{ij} for the normalized pixel value.

sensors. However, as with the raw spectral bands, very strong multicollinearity effects were observed for all three models [Fig. 5(c)] due to a strong correlation among the band ratios.

In summary, the attempts to estimate biomass using simple spectral bands of AVNIR-2 and SPOT-5 with different combinations of band ratios and PCA produced only ca. 60% usable accuracy. The reasons for this can be explained as follows.

1) The field biomass in this study area is very high (52–530 t/ha).
2) Although the near-infrared reflectance from a single leaf layer increases initially with increasing leaf cover, as

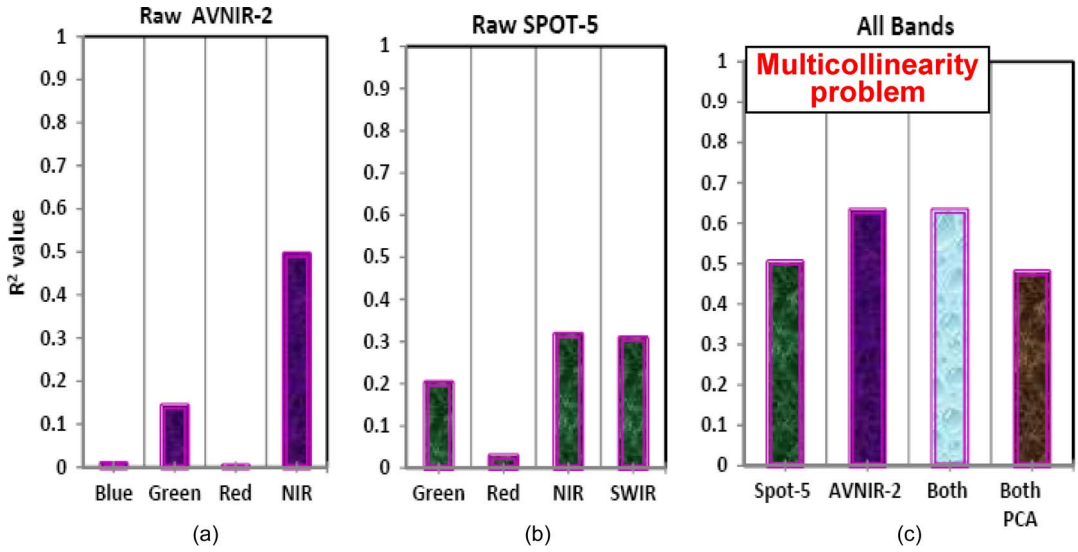

Fig. 4. Accuracy of biomass estimation using raw data.

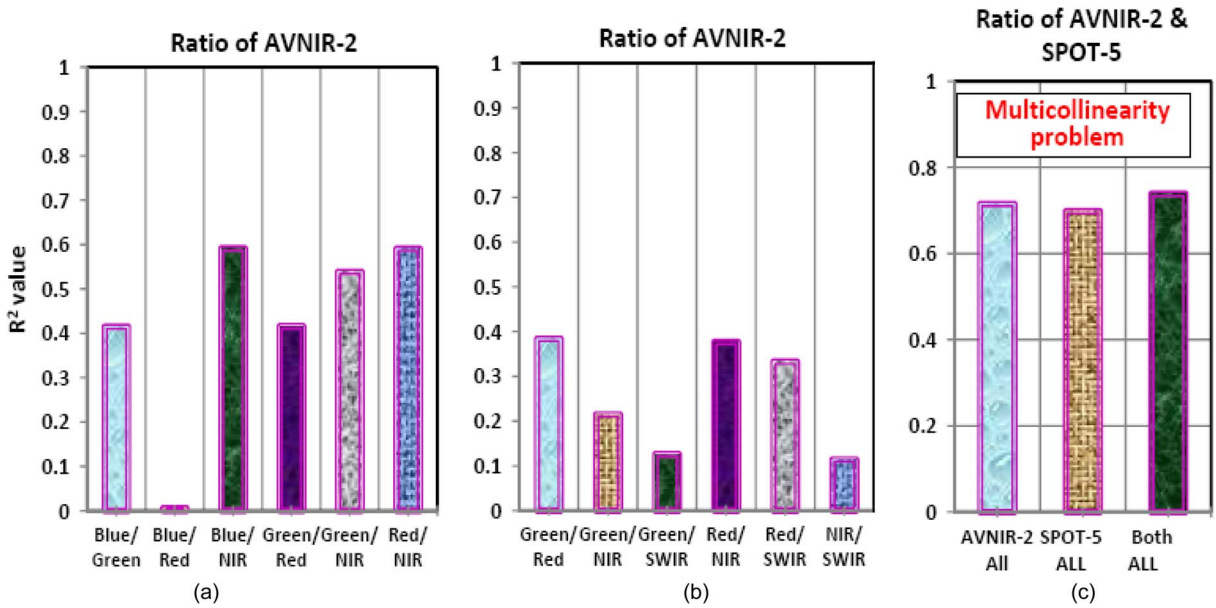

Fig. 5. Accuracy of biomass estimation using a simple ratio of raw data.

additional leaf layers are added to a canopy, these increases are not sustained [153]. Concurrently, as the canopy matures, creating more layers and increasing in complexity, shadowing acts as a spectral trap for incoming energy and reduces the amount of radiation returning to the sensor [87], [154]. This is a normal situation in tropical and subtropical forests with high biomass. A lower accuracy was also found using simple spectral bands in linear regression in many other studies [25], [26], [28], [31], [36], [80]–[82].

3) Although we used 8 spectral bands and 12 simple band ratios from the two sensors, almost all bands and ratios were highly correlated, and as a result, the multiple regression model was found to be unsuitable because of the violation of the assumption of uncorrelated independent variables [25]. Hence, we were unable to take advantage of the potential synergies between the different sensors for biomass estimation.
4) Ratios and vegetation indices have been shown to be mainly useful in temperate and boreal forest regions [5], [37], [88], [96], [155]–[158], where forests have a relatively simple structure. In tropical and subtropical regions, the forest structure is very complex, and the relationship between the vegetation index and biomass is asymptotic [25], [159], especially in tropical forests with high biomass.

Considering the moderate accuracy obtained so far, this paper decided to investigate further using the spatial characteristics of the images, particularly texture, for biomass estimation. Texture is an important variable, and it has already shown potential for biomass estimation using optical data [5], [38], [89], [115]–[118], [160].

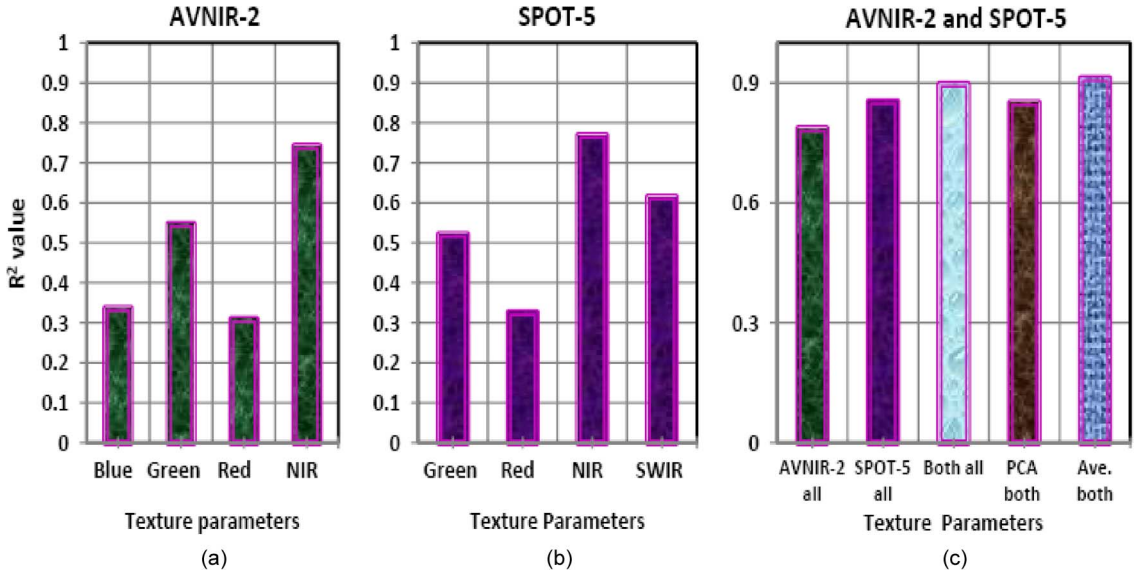

Fig. 6. Accuracy of biomass estimation using the texture parameters.

B. Performance of Texture Processing

A notable improvement was observed for both optical sensors using the texture parameters (Fig. 6(a)–(c) and models 1–5 in Table V) compared to the raw data processing [Fig. 4(a)–(c)] and simple ratios [Fig. 5(a)–(c)]. As with the raw data processing, the best ($r^2 = 0.742$ for ANVIR and $r^2 = 0.769$ for SPOT-5) and poorest ($r^2 = 0.309$ for ANVIR and $r^2 = 0.326$ for SPOT-5) results for texture were obtained from the texture parameters of the NIR and red bands, respectively, although the performance was much higher for texture measurement. Moreover, as with the raw data, the second highest performances ($r^2 = 0.547$ for ANVIR and $r^2 = 0.615$ for SPOT-5) were also obtained from the green and SWIR bands using the AVNIR-2 and SPOT-5 data, respectively. These patterns of improvement were consistent for both sensors and very much in agreement with the general behavior of the interaction between different wavelengths and vegetation. Thus, we found that texture measurement enhanced biomass estimation across all bands, but a greater improvement was observed from the bands where reflectance from vegetation is higher.

Furthermore, the texture parameters from all bands together (all bands of either AVNIR-2 or SPOT-5) were found to be very useful, with r^2 of 0.786 [rmse $= 46.53$ for AVNIR-2; model 1 in Table V and Fig. 6(c)] and 0.854 [rmse $= 38.54$ for SPOT-5; model 2 in Table V and Fig. 6(c)], which were higher than any previous processing steps. Apart from these improvements the models (using all texture parameters of an individual sensor together) were significant, and no multicollinearity effects were evident (models 1 and 2 in Table V). Generally, the best results were obtained using window sizes of 3×3 and 5×5, as well as all window sizes (3×3 to 9×9) combined, and this is thought to be due to the over-smoothing of the textural variations by the larger window sizes as well as their dissimilarity to the 30-m diameter field plots.

In addition to the single band texture parameters and all texture parameters of an individual sensor together, three different approaches combining the texture parameters of both sensors were used to estimate the biomass. These included all texture parameters from both sensors together in the model, all texture parameters of PCA of both sensors together, and all texture parameters from the averaging of both sensors together.

A very significant improvement was obtained from this processing, although PCA was not found to be very effective. The highest ($r^2 = 0.911$ and rmse $= 30.10$) and the second best ($r^2 = 0.897$ and rmse $= 32.38$) results were obtained from the texture parameters from the averaging of both sensors [model 5 in Table V and Fig. 6(c)] and from the texture parameters of both sensors in the model, respectively [model 4 in Table V and Fig. 6(c)]. These results were considerably better considering r^2, rmse, p-level (model and all variables), and multicollinearity effects. The models were significant, and multicollinearity effects were not noted. The relationships between the field biomass and the best five model predicted biomass, comprising all texture parameters from AVNIR-2 [Fig. 7(a)], SPOT-5 [Fig. 7(b)], both sensors together [Fig. 7(c)], PCA of both sensors [Fig. 7(d)], and the average of both sensors [Fig. 7(e)], also demonstrated very good agreements for model fitting (Fig. 7), although the performance varies among these models. The lowest rmse (30.10) was observed from the averaged texture parameters of both sensors [model 5 in Table V and Fig. 7(e)], while the highest rmse (46.53) was observed from the model using all texture parameters of AVNIR-2 data [model 1 in Table V and Fig. 7(a)]. These differences were attributed to the fact that averaging is a type of data fusion, and the synergy between the two sensors probably contributed complementary information in the model [model 5 in Table V and Fig. 7(e)].

The following observations arise from the results.

1) Biomass estimation was improved using the texture parameters of AVNIR-2 and SPOT-5, and this was very

TABLE V
RESULTS OF BIOMASS ESTIMATION USING THE TEXTURE PARAMETERS

Data	Model Parameters					Parameters for Intercept and Variables							
	R	R^2	A.R^2	RMSE	p-level	Variables & intercept	B	Err. of B	p-level	Tol	VIF	EV	CI
Model-1	.887	.786	.757	46.53	.000	Intercept	462.67	58.16	.000				
Texture parameters of						ME_AB4_5	-13.32	2.47	.000	.665	1.50	.978	2.31
AVNIR-2 all bands						Ku_AB2_9	12.46	2.57	.000	.728	1.37	.376	3.73
						CO_AB4_9	10.37	2.57	.000	.823	1.21	.233	4.74
						EN_AB3_9	-58.13	15.53	.001	.773	1.29	.106	7.04
						Sk_AB2_5	51.01	15.81	.002	.660	1.51	.042	11.12
						Sk_AB1_9	-23.91	10.57	.029	.674	1.48	.008	25.58
Model-2	.924	.854	.833	38.54	.000	Intercept	138.71	45.63	.004				
Texture parameters of						Sk_SB3_9	81.61	11.64	.000	.589	1.69	1.13	2.21
SPOT-5 all bands						ASM_SB1_9	456.44	97.21	.000	.491	2.03	.212	5.10
						HO_SB4_9	-312.72	96.09	.002	.210	4.75	.056	9.95
						ID_SB3_5	242.48	59.82	.000	.934	1.07	.035	12.56
						ID_SB2_3	-227.56	69.01	.002	.798	1.25	.014	19.78
						GASM_SB4_5	434.75	88.40	.000	.269	3.71	.008	26.69
Model-3	.947	.897	.879	32.38	.000	Intercept	247.95	45.53	.000				
Texture parameters of						ASM_SB1_9	499.26	73.92	.000	.614	1.62	1.28	2.13
both sensors						ASM_AB4_9	1800.07	246.45	.000	.287	3.47	.335	4.16
						HO_AB4_7	-394.39	83.93	.000	.288	3.47	.286	4.50
						Sk_SB3_7	60.11	12.67	.000	.593	1.68	.157	6.09
						Var_SB3_9	.207	.051	.000	.530	1.88	.100	7.64
						GEN_SB4_7	-83.08	24.06	.001	.383	2.61	.019	17.38
						MED_AB3_5	54.78	25.08	.035	.732	1.36	.007	28.11
Model-4	.922	.851	.826	38.80	.000	Intercept	105.21	31.74	.002				
Texture parameters from						ASM_BPC1_9	578.77	154.14	.001	.320	3.12	1.43	1.89
PCA both sensors						CO_BPC3_9	.648	.207	.003	.783	1.27	.850	2.45
						Sk_BPC1_7	80.92	15.45	.000	.501	1.99	.269	4.36
						Var_BPC2_9	-.278	.052	.000	.631	1.58	.138	6.09
						Var_BPC1_9	.175	.055	.003	.428	2.33	.133	6.21
						Std_BPC1_5	-50.63	14.71	.001	.259	3.85	.038	11.58
						MED_BPC3_3/4_3	64.05	24.28	.012	.450	2.22	.019	16.62
Model-5	.954	.911	.896	30.10	.000	Intercept	107.41	27.78	.000				
Texture parameters from						Ku_A4+S4_7	33.17	4.94	.000	.529	1.88	1.26	2.14
the Averaging of both						ASM_A2+S1_9	134.41	47.19	.007	.562	1.78	.328	4.21
sensors						Ku_A2+S1_5	-19.61	4.95	.000	.832	1.20	.279	4.56
						Sk_A4+S3_7	91.83	9.96	.000	.596	1.67	.142	6.40
						Var_A4+S3_9	.285	.119	.021	.798	1.25	.092	7.93
						ASM_A4+S3_9	937.03	277.5	.002	.456	2.19	.052	10.5
						HO_A3+S2_3	-127.63	51.74	.018	.633	1.58	.019	17.3

much expected, as previous studies using optical [5], [38] and SAR data [42], [51], [53], [161] also observed better biomass estimation using texture because of its ability to reduce the complexity of the forest structure.

2) In this paper, we observed that texture measurement improved biomass estimation for every single band, compared to the spectral reflectance of that band, and this improvement was very much correlated with the magnitude of the vegetation response to individual bands.
3) The texture parameters of a single band or all bands from a sensor, or from both sensor can be used effectively in multiple regression models because of the ability of different texture algorithms and multiple window sizes to produce uncorrelated texture parameters, which is

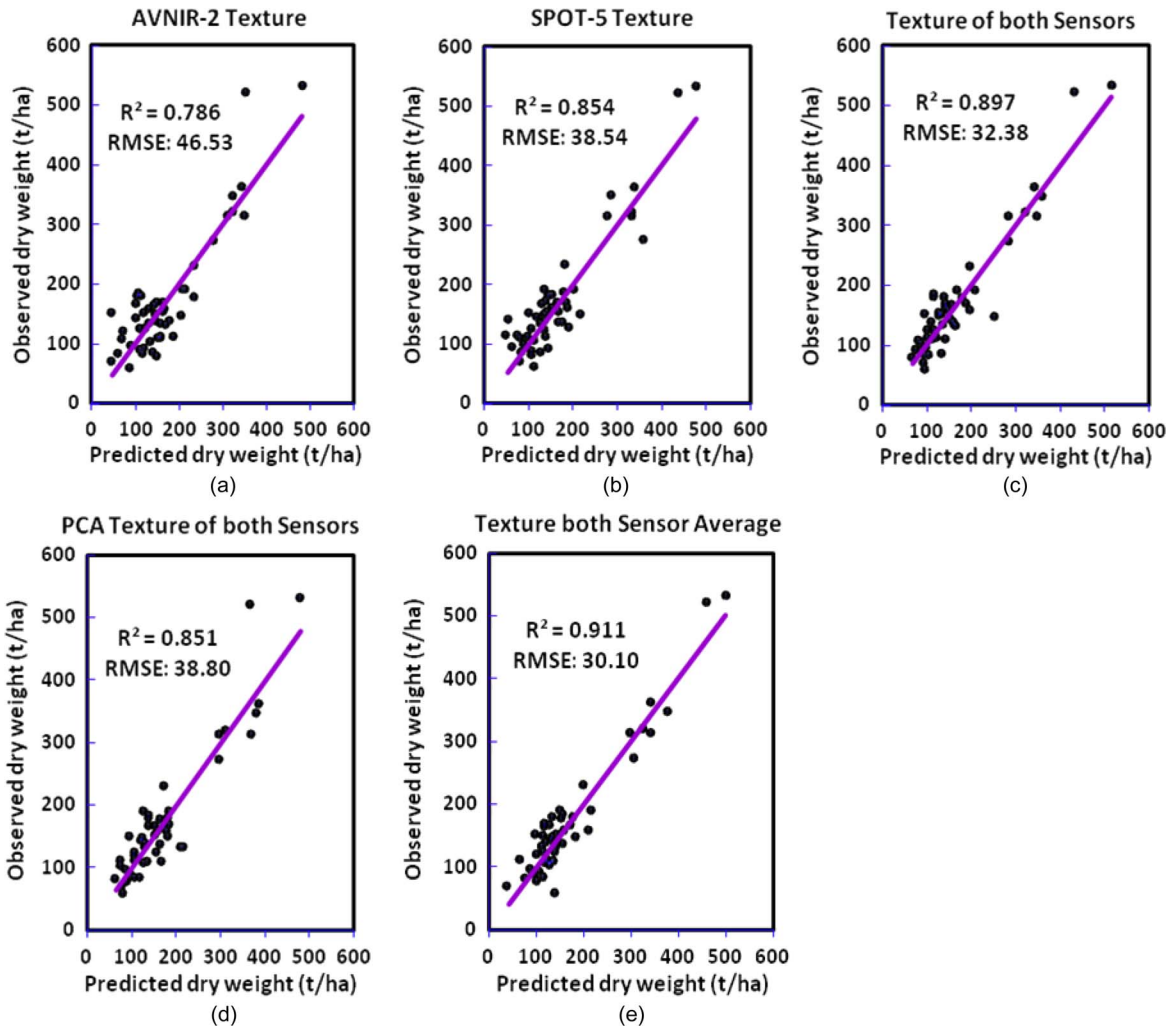

Fig. 7. Relationships between the field biomass and the model-predicted biomass using different combinations of texture parameters.

essential in maintaining the assumption of uncorrelated independent variables for the development of multiple regression models. This was not observed in the case of spectral reflectance because of the strong correlation between the different bands [25].

4) As with the raw data, we observed that PCA was not very effective because, even though most information is present on the resulting compressed components, there is some information loss, and because the standard PCA procedure is unable to distinguish the input variables that are useful for biomass estimation from those that are not.
5) All texture parameters from both sensors together were found to be very effective, and they obtained ca. 90% agreement ($r^2 = 0.897$) for biomass estimation probably because of the fact that different sensors have the ability to provide at least some complementary information which may provide uncorrelated independent variables in the model. This type of complementary information has normally been applied to the SAR data using the data of different polarizations and frequencies [66], [84], [162] and also in multisensor approaches where complementary information was obtained from different sensors [18], [19], [74].
6) The best estimate ($r^2 = 0.911$ and rmse $= 30.10$) was achieved from the averaged texture parameters of both sensors (model 5 in Table V). Averaging is a basic data fusion method, and the texture parameters of the averaged images have never been used with optical sensors for biomass estimation. Previous work with SAR data has showed that the use of several different dates of SAR by averaging or other means can provide more reliable results than a single SAR image due to the reduction of speckle noise and other random errors [46], [47], [163]. In general, the results suggest that this type of averaging can be applied to optical images to reduce the rmse and to improve the accuracy of biomass estimation.

Although the texture measurement of both sensors together, either averaged (model 5 in Table V) or together in the model (model 3 in Table V), was able to produce a robust model for biomass estimation, this paper still decided to investigate further. Given the fact that band ratios have the ability to reduce many unwanted problems such as topographic, forest structural,

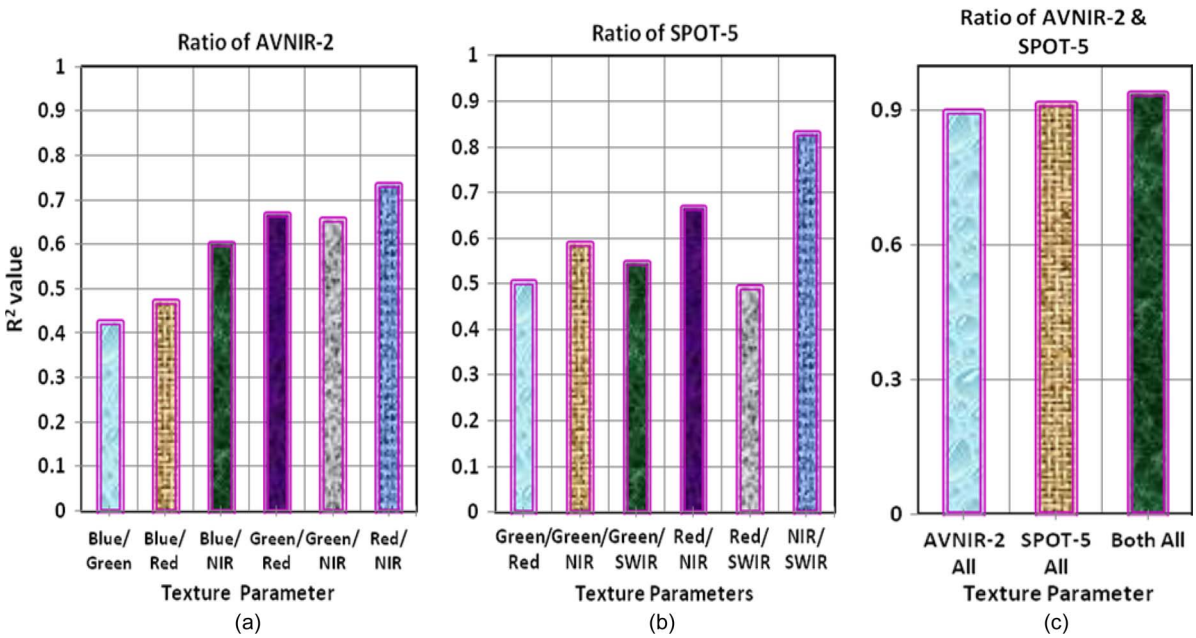

Fig. 8. Accuracy of biomass estimation using the ratio of the texture parameters in different combinations.

atmospheric, soil background, and solar irradiance effects, the simple band ratio of the texture parameters was examined.

C. Ratio of the Texture Parameters

The ratio of the texture parameters was found to be very effective for biomass estimation compared to the best results obtained from all previous steps (Fig. 9). The accuracies obtained (Fig. 8) using all simple ratios of the texture parameters of AVNIR-2 ($r^2 = 0.899$ and rmse $= 32.04$), SPOT-5 ($r^2 = 0.916$ and rmse $= 29.09$), and both sensors together ($r^2 = 0.939$ and rmse $= 24.77$) were considerably higher than the results obtained from all texture parameters of AVNIR-2 ($r^2 = 0.786$ and rmse $= 46.53$), SPOT-5 ($r^2 = 0.854$ and rmse $= 38.54$), and both sensors ($r^2 = 0.911$ and rmse $= 30.10$) (Fig. 9). Similar to the texture models, no multicollinearity effects were evident for the models (models 1, 2, and 3 in Table VI) whether from a single sensor (either AVNIR-2 or SPOT-5) or both sensors together. All three models were significant, and fitted the field data very well (Fig. 10). However, the best fit between the model-predicted biomass and the field biomass was observed using the ratio of the texture parameters of both sensors together (Fig. 10(c) and model 3 in Table VI). The lowest rmse (24.77) and the highest r^2 (0.939) of this model (model 3 in Table VI) made it outstanding in performance compared to the other models, with very strong potential for biomass estimation.

This great improvement in biomass estimation can be explained by the fact that, at this stage, we used three image processing techniques together as follows.

1) Texture processing which had already shown a potential for biomass estimation in many previous studies using optical [5], [38] and SAR data [42], [51], [53], [161]. This paper found (Section IV-B) that texture processing can greatly enhance the accuracy of biomass estimation compared to the spectral reflectance and the simple ratio of the spectral reflectance.
2) Data sets from two different sensors (AVNIR-2 and SPOT-5) were used in this processing. Although both data sets are from optical sensors, there are differences in the wavebands. Therefore, it was anticipated that at least some complementary information could be obtained. The use of different sensors (e.g., optical and SAR; optical, SAR, and lidar; high-resolution optical with low-resolution optical; panchromatic and multispectral optical; different polarizations of SAR; and different frequencies of SAR) are already proven to be effective for

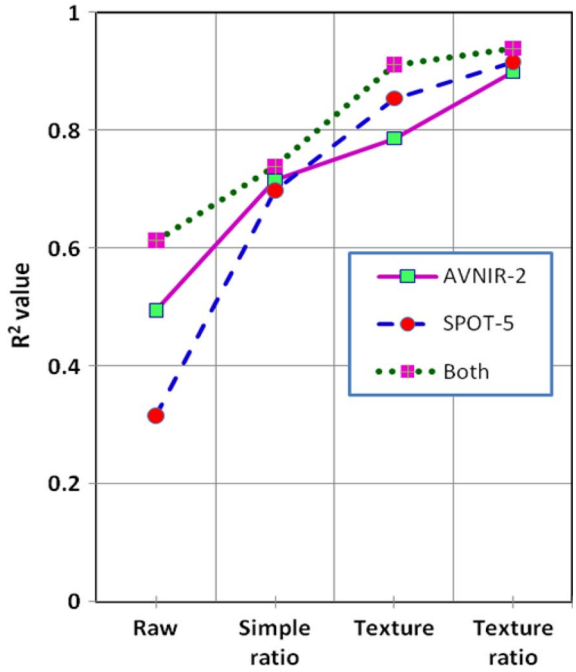

Fig. 9. Change in the accuracy of the biomass estimation among raw, simple band ratios, image textures, and ratios of the image texture.

TABLE VI
RESULTS OF THE BIOMASS ESTIMATION USING THE RATIO OF THE TEXTURE PARAMETERS

Data	Model Parameters					Parameters for Intercept and Variables							
	R	R2	A.R2	RMSE	p-level	Variables & intercept	B	Std. Err. of B	p-level	Tol	VIF	EV	CI
Model-1 Texture parameter ratio of AVNIR-2	.948	.899	.879	32.04	.000	Intercept	118.49	39.31	.004				
						GEN_AT1/4_9	-112.38	34.47	.002	.617	1.62	.430	4.32
						ASM_AT2/3_7	-84.38	26.61	.003	.379	2.63	.187	6.56
						GEN_AT2/3_7	-50.45	15.74	.003	.475	2.10	.128	7.91
						DI_AT2/3_9	107.88	17.26	.000	.590	1.69	.076	10.28
						Std_AT2/4_5	-134.78	27.96	.000	.340	2.94	.067	10.93
						ME_AT2/4_9	-1327.87	102.30	.000	.384	2.60	.034	15.33
						ME_AT3/4_9	1296.57	95.64	.000	.240	4.16	.020	20.07
						Ku_ST2/3_5	58.74	10.68	.000	.680	1.47	.012	26.36
Model-2 Texture parameter ratio of SPOT-5	.957	.916	.903	29.09	.000	Intercept	73.43	29.84	.018				
						Sk_ST3/4_9	7615.2	710.7	.000	.715	1.39	1.17	2.24
						DI_ST2/4_7	15.82	2.24	.000	.607	1.64	.430	3.70
						Var_ST3/4_9	39.95	7.80	.000	.227	4.40	.213	5.27
						ASM_ST1/2_5	18.58	3.79	.000	.530	1.88	.192	5.54
						MED_ST3/4_7	-1217.5	304.5	.000	.222	4.49	.065	9.55
						CO_ST2/4_9	-8.56	2.24	.000	.304	3.29	.013	21.1
						GEN_ST3/4_9	63.95	20.93	.004	.335	2.98	.010	24.7
Model-3 Texture parameter ratio of both sensors	.969	.939	.926	24.77	.000	Intercept	80.70	27.70	.006				
						DI_ST2/4_7	13.03	2.21	.000	.474	2.11	1.23	2.46
						Sk_ST3/4_9	7616.2	631.2	.000	.690	1.44	.462	4.02
						Var_ST3/4_9	35.41	6.91	.000	.220	4.54	.254	5.43
						ASM_ST1/2_5	21.15	3.43	.000	.492	2.03	.229	5.71
						MD_ST3/4_7	-1136.1	266.8	.000	.221	4.53	.157	6.90
						CO_ST2/4_9	-11.11	2.08	.000	.268	3.73	.118	7.95
						GEN_ST3/4_9	81.78	18.82	.000	.315	3.17	.042	13.42
						MED_aT2/3_5	-26.48	7.31	.001	.766	1.30	.012	24.55
						CO_AT2/3_7	24.21	11.71	.045	.702	1.42	.010	27.88

biomass estimation because it provides complementary information [18], [19], [46], [47], [74], [163]

3) Finally, we tested the ratio of the texture parameters. We know from previous research that ratios, whether simple or complex and whether between different bands, polarizations, or frequencies, can improve biomass estimation by minimizing the features which are similar in both bands, such as topographic and forest structural effects. This ratio effect has been shown using both optical [90]–[93]; [119]; [146]–[152] and SAR data [21], [66], [69], [71], [72], [164]. Thus, we found (Section IV-B) as with previous research using optical [5], [38] and SAR data [42], [51], [53], [161], that texture parameters have the ability to improve biomass estimation, and it is reasonable to believe that the ratio of the texture parameters would be able to further improve biomass estimation because of the combination of two well-proven image processing techniques.

V. DISCUSSION

A very promising accuracy ($r^2 = 0.939$ and rmse $= 24.77$) for biomass estimation was achieved from the combined processing of texture, ratio, and complementary sensor information from two optical sensors (AVNIR-2 and SPOT-5). Using the raw data, only moderate performance $(r^2 = 0.494)$ was observed from the spectral reflectance of NIR of the AVNIR-2 data. This was expected as the biomass of this study area is very high, and in tropical and subtropical regions, reflectance is not linearly related to biomass because of the complex canopy layers and heterogeneous vegetation structures [87], [154]. A somewhat better result $(r^2 = 0.631)$ was obtained from the simple ratio of the red/NIR data compared to the raw spectral reflectance. The still only moderate performance obtained from the ratio was in agreement with the findings of previous research [5], [37], [88], [96], [155]–[158], which found that ratios or vegetation indices, whether complex or simple, are mainly useful in temperate and boreal forests with

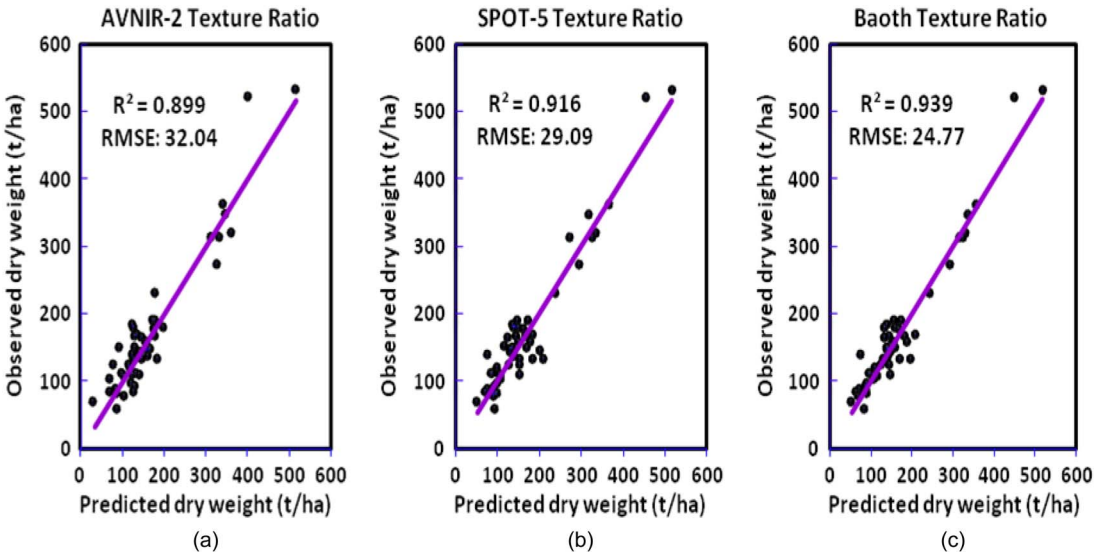

Fig. 10. Relationships between the field biomass and the model-predicted biomass using different combinations of the image texture ratios.

a relatively simple structure. In tropical and subtropical forest, ratios and vegetation indices have not been found very effective because of the complex forest structure [25], [38], [159]. Although a better result was obtained from the combinations of all raw bands together ($r^2 = 0.63$) and all simple ratios together ($r^2 = 0.739$), very strong multicollinearity effects were evident because of the high correlation among different bands and among different band ratios.

Biomass estimation was observed to improve considerably when texture parameters were used in the model. This improvement was noted for all stages of processing, including single bands, all bands of a single sensor together, and all bands of both sensors together. Promising results were obtained from all texture parameters of AVNIR-2 ($r^2 = 0.786$) and SPOT-5 ($r^2 = 0.854$), and this was further improved when the texture parameters of both sensors were used in the model ($r^2 = 0.911$). The improvement of biomass estimation using texture parameters was very much anticipated, and our results comply with other findings of higher accuracy using texture measurements of optical [5], [38] and SAR data [42], [51], [53], [161], compared to raw spectral reflectance or backscattering. The highest agreement ($r^2 = 0.911$) obtained from the texture parameters of both sensors averaged is significantly higher than any previous study and is very promising for future work. We believe that this good result was obtained mainly because of the relatively high resolution of both sensors, as texture is more applicable to fine spatial resolution imagery [51], [61], [110], [121]–[125], as well as the complementary information from the two sensors in the averaging procedure [46], [47], [163].

After three stages of processing, three very promising accuracies were obtained. These were the ratio of the texture parameters of AVNIR-2 ($r^2 = 0.899$ and rmse $= 32.04$), the ratio of the texture parameters of SPOT-5 ($r^2 = 0.916$ and rmse $=$ 29.09), and the ratio of the texture parameters of both sensors together ($r^2 = 0.939$ and rmse $= 24.77$). The accuracies of all three models were very promising, but the performance using the ratio of the texture parameters of both sensors together superseded all other models. The accuracies obtained in this paper are very high, and result from the high-quality data (from two high-resolution optical sensors) and advanced processing techniques (averaging of two sensors, texture measurement and ratio), making us believe that this accuracy is reasonable and useful for biomass estimation in future studies and in other areas. Assuming correct image preprocessing [26], [73] and good field data, similar results should be obtainable in other study areas using similar steps to those described here. However, the precise selection of processing steps such as the ideal window sizes and texture measurements, such as GLCM-based or SADH-based, would require investigation as they depend on the biomass level, forest structure, and other environmental conditions of the study area. We suggest that the processing models presented here can be used as templates for future work.

VI. Conclusion

Although the potential of texture for biomass estimation with optical sensors has previously been demonstrated, only low to moderate agreements of below $r^2 = 0.65$ have been achieved. The very high agreements obtained between field and model biomass from the texture parameters of both SPOT-5 and AVNIR-2 sensors together, as well as for the ratio of the texture parameters, were achieved in spite of the challenging nature of the study area in a complex subtropical forested region. This very promising result is surprising to the researchers, but one possible explanation would be the comprehensive and study-area-specific nature of the field biomass data and the demonstrated good fit of the allometric model (i.e., r^2 of 0.93) devised for this paper from the destructive sampling of 75 trees. The accuracy of locating the field biomass plots was also ensured by their large size (15-m radius), compared with an image resolution of 10 m, as well as by the detailed knowledge of the study area by the researchers.

Along with the high-quality field data, a combination of image processing techniques was devised to exploit both the spectral and spatial characteristics of two advanced fine-resolution

optical sensors. In particular, the high (10 m) image resolutions of SPOT-5 and AVNIR-2, compared to the 30-m resolution of Landsat used in most previous biomass estimations, has enabled measurement of local variance in the forest structure, with crown sizes similar to the image resolution. In such a case, reflectance differences between individual trees and their background, as well as between different tree species, are maximized, resulting in a high local variance [130]. Apart from the advantages of high resolution, texture measurement can maximize the discrimination of spatial information independently from tone and can increase the biomass range that can be measured, as well as reduce those forest structural differences which are independent of biomass, while the image ratios are able to cancel out the background effects which register a similar response in both bands, such as inequalities in solar illumination, observation angle, and shadow. A further reduction of the unwanted background information may have been achieved by the averaging of two sensors, which is an approach that has proven successful in SAR images for the mitigation of random error and sensor noise. Finally, the complementary bands of SPOT-5 and AVNIR-2, namely, blue (AVNIR-2) and SWIR (SPOT-5), were able to supplement the information from the common green, red, and NIR bands, altogether resulting in a very promising result for biomass estimation using two high-resolution optical sensors.

ACKNOWLEDGMENT

The authors would like to thank the Hong Kong Agriculture, Fisheries and Conservation Department for their help with the tree harvesting in the country parks and the Japan Aerospace Exploration Agency for the ALOS images, under ALOS agreement no. 376.

REFERENCES

[1] COP15, United Nations Climate Change Conference in Copenhagen 2009 (22, December), Jan. 15, 2010.

[2] P. W. West, *Tree and Forest Measurement,* 2nd ed. Berlin, Germany: Springer-Verlag, 2009.

[3] D. Skole and C. Tucker, "Tropical deforestation and habitat fragmentation in the Amazon: Satellite data from 1978 to 1988," *Science*, vol. 260, no. 5116, pp. 1905–1910, Jun. 1993.

[4] P. Muukkonen and J. Heiskanen, "Estimating biomass for boreal forests using ASTER satellite data combined with standwise forest inventory data," *Remote Sens. Environ.*, vol. 99, no. 4, pp. 434–447, Dec. 2005.

[5] H. Fuchs, P. Magdon, C. Kleinn, and H. Flessa, "Estimating aboveground carbon in a catchment of the Siberian forest tundra: Combining satellite imagery and field inventory," *Remote Sens. Environ.*, vol. 113, no. 3, pp. 518–531, Mar. 2009.

[6] D. H. Alban, D. A. Perala, and B. E. Schlaegel, "Biomass and nutrient distribution in aspen, pine, and spruce stands on the same soil type in Minnesota," *Can. J. For. Res.*, vol. 8, pp. 290–299, 1978.

[7] T. R. Crow, "Biomass and production in three contiguous forests in Northern Wisconsin," *Ecology*, vol. 59, no. 2, pp. 265–273, Mar. 1978.

[8] S. Brown, "Tropical forests and the global carbon cycle: The need for sustainable land-use patterns," *Agric. Ecosyst. Environ.*, vol. 46, no. 1–4, pp. 31–44, Sep. 1993.

[9] D. L. Skole, W. H. Chomentowski, W. A. Salas, and A. D. Nobre, "Physical and human dimensions of deforestation in Amazonia," *Bioscience*, vol. 44, no. 5, pp. 314–322, May 1994.

[10] G. Sun and J. K. Ranson, "Forest biomass retrieval from lidar and radar," in *Proc. IGARSS*, 2009, vol. 5, pp. 300–303.

[11] S. Ryu, J. Chen, T. R. Crow, and S. C. Saunders, "Available fuel dynamics in nine contrasting forest ecosystems in North America," *Environ. Manage.*, vol. 33, no. 1, pp. S87–S107, Jul. 2004.

[12] J. Cihlar, S. Denning, F. Ahern, O. Arino, A. Belward, F. Bretherton, W. Cramer, G. Dedieu, C. Field, R. Francey, R. Gommes, J. Gosz, K. Hibbard, T. Igarashi, P. Kabat, D. Olson, S. Plummer, I. Rasool, M. Raupach, R. Scholes, J. Townshend, R. Valentini, and D. Wickland, "Initiative to quantify terrestrial carbon sources and sinks," *Eos, Trans. Amer. Geophys. Union*, vol. 83, no. 1, pp. 1–7, 2002.

[13] Å. Rosenqvist, A. Milne, R. Lucas, M. Imhoff, and C. Dobson, "A review of remote sensing technology in support of the Kyoto Protocol," *Environ. Sci. Policy*, vol. 6, no. 5, pp. 441–455, Oct. 2003.

[14] Q. M. Ketterings, R. Coe, M. Van Noordwijk, Y. Ambagau', and C. A. Palm, "Reducing uncertainty in the use of allometric biomass equations for predicting above-ground tree biomass in mixed secondary forests," *For. Ecol. Manage.*, vol. 146, no. 1–3, pp. 199–209, Jun. 2001.

[15] M. Keller, M. Palace, and G. Hurtt, "Biomass estimation in the Tapajos National Forest, Brazil: Examination of sampling and allometric uncertainties," *For. Ecol. Manage.*, vol. 154, no. 3, pp. 371–382, Dec. 2001.

[16] D. Zianis and M. Mencuccini, "On simplifying allometric analyses of forest biomass," *For. Ecol. Manage.*, vol. 187, no. 2/3, pp. 311–332, Jan. 2004.

[17] K. S. Murali, D. M. Bhat, and N. H. Ravindranath, "Biomass estimation equations for tropical deciduous and evergreen forests," *Int. J. Agric. Resour., Governance Ecol.*, vol. 4, pp. 81–92, 2005.

[18] P. Hyde, R. Dubayah, W. Walker, J. B. Blair, M. Hofton, and C. Hunsaker, "Mapping forest structure for wildlife habitat analysis using multi-sensor (lidar, SAR/InSAR, ETM+, Quickbird) synergy," *Remote Sens. Environ.*, vol. 102, no. 1/2, pp. 63–73, May 2006.

[19] P. Hyde, R. Nelson, D. Kimes, and E. Levine, "Exploring lidar–radar synergy—Predicting aboveground biomass in a southwestern ponderosa pine forest using lidar, SAR and InSAR," *Remote Sens. Environ.*, vol. 106, no. 1, pp. 28–38, Jan. 2007.

[20] S. Brown, A. J. R. Gillespie, and A. E. Lugo, "Biomass estimation methods for tropical forests with applications to forest inventory data," *Forest Sci.*, vol. 35, no. 4, pp. 881–902, Dec. 1989.

[21] T. Le Toan, A. Beaudoin, J. Riom, and D. Guyon, "Relating forest biomass to SAR data," *IEEE Trans. Geosci. Remote Sens.*, vol. 30, no. 2, pp. 403–411, Mar. 1992.

[22] S. Brown, C. A. S. Hall, W. Knabe, J. Raich, M. C. Trexler, and P. Woomer, "Tropical forests: Their past, present, and potential future role in the terrestrial carbon budget," *Water Air Soil Pollut.*, vol. 70, no. 1–4, pp. 71–94, 1993.

[23] R. K. Dixon, S. Brown, R. A. Houghton, A. M. Solomon, M. C. Trexler, and J. Wisniewski, "Carbon pools and flux of global forest ecosystems," *Science*, vol. 263, no. 5144, pp. 185–190, Jan. 1994.

[24] R. A. Houghton, D. L. Skole, C. A. Nobre, J. L. Hackler, K. T. Lawrence, and W. H. Chomentowski, "Annual fluxes of carbon from deforestation and regrowth in the Brazilian Amazon," *Nature*, vol. 403, no. 6767, pp. 301–304, Jan. 2000.

[25] G. M. Foody, M. E. Cutler, J. McMorrow, D. Pelz, H. Tangki, D. S. Boyd, and I. Douglas, "Mapping the biomass of Bornean tropical rain forest from remotely sensed data," *Glob. Ecol. Biogeogr.*, vol. 10, no. 4, pp. 379–387, Jul. 2001.

[26] G. M. Foody, D. S. Boyd, and M. E. J. Cutler, "Predictive relations of tropical forest biomass from Landsat TM data and their transferability between regions," *Remote Sens. Environ.*, vol. 85, pp. 463–474, 2003.

[27] T. Häme, A. Salli, K. Andersson, and A. Lohi, "A new methodology for the estimation of biomass of conifer-dominated boreal forest using NOAA AVHRR data," *Int. J. Remote Sens.*, vol. 18, no. 15, pp. 3211–3243, Oct. 1997.

[28] R. Salvador and X. Pons, "On the reliability of Landsat TM for estimating forest variables by regression techniques: A methodological analysis," *IEEE Trans. Geosci. Remote Sens.*, vol. 36, no. 6, pp. 1888–1897, Nov. 1998.

[29] L. Min, J. J. Qu, and H. Xianjun, "Estimating aboveground biomass for different forest types based on Landsat TM measurements," in *Proc. Geoinformatics*, 2009, pp. 1–6.

[30] D. S. Boyd, G. M. Foody, and P. J. Curran, "The relationship between the biomass of Cameroonian tropical forests and radiation reflected in middle infrared wavelengths (3.0–5.0 μm)," *Int. J. Remote Sens.*, vol. 20, no. 5, pp. 1017–1023, Mar. 1999.

[31] M. K. Steininger, "Satellite estimation of tropical secondary forest above-ground biomass: Data from Brazil and Bolivia," *Int. J. Remote Sens.*, vol. 21, no. 6/7, pp. 1139–1157, Apr. 2000.

[32] Y. Cunjian, Z. Jieming, H. He, and C. Xi, "Correlations of the biomass of the main tropical forest vegetation types and Landsat TM

data in Xishuangbanna of P. R. of China," in *Proc. IGARSS*, 2007, pp. 4336–4338.
[33] J. Dong, R. K. Kaufmann, R. B. Myneni, C. J. Tucker, P. E. Kauppi, J. Liski, W. Buermann, V. Alexeyev, and M. K. Hughes, "Remote sensing estimates of boreal and temperate forest woody biomass: Carbon pools, sources, and sinks," *Remote Sens. Environ.*, vol. 84, no. 3, pp. 393–410, Mar. 2003.
[34] T. Calvao and J. M. Palmeirim, "Mapping Mediterranean scrub with satellite imagery: Biomass estimation and spectral behaviour," *Int. J. Remote Sens.*, vol. 25, no. 16, pp. 3113–3126, Aug. 2004.
[35] O. Mutanga and A. K. Skidmore, "Narrow band vegetation indices overcome the saturation problem in biomass estimation," *Int. J. Remote Sens.*, vol. 25, no. 19, pp. 3999–4014, Oct. 2004.
[36] P. S. Thenkabail, N. Stucky, B. W. Griscom, M. S. Ashton, J. Diels, B. Van der Meer, and E. Enclona, "Biomass estimations and carbon stock calculations in the oil palm plantations of African derived savannas using IKONOS data," *Int. J. Remote Sens.*, vol. 25, no. 23, pp. 5447–5472, Dec. 2004.
[37] D. Zheng, J. Rademacher, J. Chen, T. Crow, M. Bresee, J. Le Moine, and S. Ryu, "Estimating aboveground biomass using Landsat 7 ETM+ data across a managed landscape in Northern Wisconsin, USA," *Remote Sens. Environ.*, vol. 93, no. 3, pp. 402–411, Nov. 2004.
[38] D. Lu, "Aboveground biomass estimation using Landsat TM data in the Brazilian Amazon," *Int. J. Remote Sens.*, vol. 26, no. 12, pp. 2509–2525, Jun. 2005.
[39] M. M. Rahman, E. Csaplovics, and B. Koch, "An efficient regression strategy for extracting forest biomass information from satellite sensor data," *Int. J. Remote Sens.*, vol. 26, no. 7, pp. 1511–1519, Apr. 2005.
[40] M. M. Rahman, E. Csaplovics, and B. Koch, "Satellite estimation of forest carbon using regression models," *Int. J. Remote Sens.*, vol. 29, no. 23, pp. 6917–6936, Dec. 2008.
[41] P. T. Wolter, P. A. Townsend, and B. R. Sturtevant, "Estimation of forest structural parameters using 5 and 10 meter SPOT-5 satellite data," *Remote Sens. Environ.*, vol. 113, no. 9, pp. 2019–2036, Sep. 2009.
[42] A. J. Luckman, A. C. Frery, C. C. F. Yanasse, and G. B. Groom, "Texture in airborne SAR imagery of tropical forest and its relationship to forest regeneration stage," *Int. J. Remote Sens.*, vol. 18, no. 6, pp. 1333–1349, Apr. 1997.
[43] M. L. Williams, T. Milne, I. Tapley, J. J. Reis, M. Sanford, B. Kofman, and S. Hensley, "Tropical forest biomass recovery using GeoSAR observations," in *Proc. IGARSS*, 2009, vol. 4, pp. IV-173–IV-176.
[44] J. R. Santos, C. C. Freitas, L. S. Araujo, L. V. Dutra, J. C. Mura, F. F. Gama, L. S. Soler, and S. J. S. Sant'Anna, "Airborne P-band SAR applied to the aboveground biomass studies in the Brazilian tropical rainforest," *Remote Sens. Environ.*, vol. 87, no. 4, pp. 482–493, Nov. 2003.
[45] J. R. Santos, M. S. Pardi Lacruz, L. S. Araujo, and M. Keil, "Savanna and tropical rainforest biomass estimation and spatialization using JERS-1 data," *Int. J. Remote Sens.*, vol. 23, no. 7, pp. 1217–1229, Apr. 2002.
[46] L. Kurvonen, J. Pulliainen, and M. Hallikainen, "Retrieval of biomass in boreal forests from multitemporal ERS-1 and JERS-1 SAR images," *IEEE Trans. Geosci. Remote Sens.*, vol. 37, no. 1, pp. 198–205, Jan. 1999.
[47] J. E. S. Fransson and H. Israelsson, "Estimation of stem volume in boreal forests using ERS-1 C- and JERS-1 L-band SAR data," *Int. J. Remote Sens.*, vol. 20, no. 1, pp. 123–137, Jan. 1999.
[48] T. Castel, F. Guerra, Y. Caraglio, and F. Houllier, "Retrieval biomass of a large Venezuelan pine plantation using JERS-1 SAR data. Analysis of forest structure impact on radar signature," *Remote Sens. Environ.*, vol. 79, no. 1, pp. 30–41, Jan. 2002.
[49] G. Sun, K. J. Ranson, and V. I. Kharuk, "Radiometric slope correction for forest biomass estimation from SAR data in the Western Sayani Mountains, Siberia," *Remote Sens. Environ.*, vol. 79, no. 2/3, pp. 279–287, Feb. 2002.
[50] R. Tsolmon, R. Tateishi, and J. S. S. Tetuko, "A method to estimate forest biomass and its application to monitor Mongolian taiga using JERS-1 SAR data," *Int. J. Remote Sens.*, vol. 23, no. 22, pp. 4971–4978, Nov. 2002.
[51] T. M. Kuplich, P. J. Curran, and P. M. Atkinson, "Relating SAR image texture to the biomass of regenerating tropical forests," *Int. J. Remote Sens.*, vol. 26, no. 21, pp. 4829–4854, Nov. 2005.
[52] R. M. Lucas, A. L. Mitchell, A. Rosenqvist, C. Proisy, A. Melius, and C. Ticehurst, "The potential of L-band SAR for quantifying mangrove characteristics and change: Case studies from the tropics," *Aquatic Conservation, Mar. Freshwater Ecosyst.*, vol. 17, no. 3, pp. 245–264, May 2007.
[53] I. Champion, P. Dubois-Fernandez, D. Guyon, and M. Cottrel, "Radar image texture as a function of forest stand age," *Int. J. Remote Sens.*, vol. 29, no. 6, pp. 1795–1800, Mar. 2008.
[54] K. Zhao, S. Popescu, and R. Nelson, "Lidar remote sensing of forest biomass: A scale-invariant estimation approach using airborne lasers," *Remote Sens. Environ.*, vol. 113, no. 1, pp. 182–196, Jan. 2009.
[55] M. A. Lefsky, W. B. Cohen, S. A. Acker, G. G. Parker, T. A. Spies, and D. Harding, "Lidar remote sensing of the canopy structure and biophysical properties of Douglas-fir western hemlock forests," *Remote Sens. Environ.*, vol. 70, no. 3, pp. 339–361, Dec. 1999.
[56] J. B. Drake, R. O. Dubayah, R. G. Knox, D. B. Clark, and J. B. Blair, "Sensitivity of large-footprint lidar to canopy structure and biomass in a neotropical rainforest," *Remote Sens. Environ.*, vol. 81, no. 2, pp. 378–392, Aug. 2002.
[57] G. Patenaude, R. A. Hill, R. Milne, D. L. A. Gaveau, B. B. J. Briggs, and T. P. Dawson, "Quantifying forest above ground carbon content using lidar remote sensing," *Remote Sens. Environ.*, vol. 93, no. 3, pp. 368–380, Nov. 2004.
[58] Z. J. Bortolot and R. H. Wynne, "Estimating forest biomass using small footprint lidar data: An individual tree-based approach that incorporates training data," *ISPRS J. Photogramm. Remote Sens.*, vol. 59, no. 6, pp. 342–360, Nov. 2005.
[59] M. A. Wulder, R. J. Hall, N. C. Coops, and S. E. Franklin, "High spatial resolution remotely sensed data for ecosystem characterization," *Bioscience*, vol. 54, no. 6, pp. 511–521, Jun. 2004.
[60] D. Lu, "The potential and challenge of remote sensing-based biomass estimation," *Int. J. Remote Sens.*, vol. 27, no. 7, pp. 1297–1328, Apr. 2006.
[61] D. S. Boyd and F. M. Danson, "Satellite remote sensing of forest resources: Three decades of research development," *Prog. Phys. Geogr.*, vol. 29, no. 1, pp. 1–26, Jan. 2005.
[62] E. Tomppo, M. Nilsson, M. Rosengren, P. Aalto, and P. Kennedy, "Simultaneous use of Landsat-TM and IRS-1C WiFS data in estimating large area tree stem volume and aboveground biomass," *Remote Sens. Environ.*, vol. 82, no. 1, pp. 156–171, Sep. 2002.
[63] E. Nezry, E. Mougin, A. Lopes, J. P. Gastellu-Etchegorry, and Y. Laumonier, "Tropical vegetation mapping with combined visible and SAR spaceborne data," *Int. J. Remote Sens.*, vol. 14, no. 11, pp. 2165–2184, Jul. 1993.
[64] P. Mayaux, G. De Grandi, and J. Malingreau, "Central African forest cover revisited: A multisatellite analysis," *Remote Sens. Environ.*, vol. 71, no. 2, pp. 183–196, Feb. 2000.
[65] S. Wu, "Potential application of multipolarization SAR for pine-plantation biomass estimation," *IEEE Trans. Geosci. Remote Sens.*, vol. GRS-25, no. 3, pp. 403–409, May 1986.
[66] K. J. Ranson and G. Sun, "Mapping biomass of a northern forest using multifrequency SAR data," *IEEE Trans. Geosci. Remote Sens.*, vol. 32, no. 2, pp. 388–396, Mar. 1994.
[67] G. Sandberg, L. M. H. Ulander, J. E. S. Fransson, J. Holmgren, and T. Le Toan, "Comparison of L- and P-band biomass retrievals based on backscatter from the BioSAR campaign," in *Proc. IGARSS*, 2009, vol. 4, pp. 169–172.
[68] M. C. Dobson, F. T. Ulaby, T. LeToan, A. Beaudoin, E. S. Kasischke, and N. Christensen, "Dependence of radar backscatter on coniferous forest biomass," *IEEE Trans. Geosci. Remote Sens.*, vol. 30, no. 2, pp. 412–415, Mar. 1992.
[69] C. M. Dobson, F. T. Ulaby, L. E. Pierce, T. L. Sharik, K. M. Bergen, J. Kellndorfer, J. R. Kendra, E. Li, Y. C. Lin, A. Nashashibi, K. Sarabandi, and P. Siqueira, "Estimation of forest biophysical characteristics in Northern Michigan with SIR-C/X-SAR," *IEEE Trans. Geosci. Remote Sens.*, vol. 33, no. 4, pp. 877–895, Jul. 1995.
[70] E. S. Kasischke, N. L. Christensen, Jr., and L. L. Bourgeau-Chavez, "Correlating radar backscatter with components of biomass in loblolly pine forests," *IEEE Trans. Geosci. Remote Sens.*, vol. 33, no. 3, pp. 643–659, May 1995.
[71] P. A. Harrell, E. S. Kasischke, L. L. Bourgeau-Chavez, E. M. Haney, and N. L. Christensen, Jr., "Evaluation of approaches to estimating aboveground biomass in southern pine forests using SIR-C data," *Remote Sens. Environ.*, vol. 59, no. 2, pp. 223–233, Feb. 1997.
[72] G. M. Foody, R. M. Green, R. M. Lucas, P. J. Curran, M. Honzak, and I. Do Amaral, "Observations on the relationship between SIR-C radar backscatter and the biomass of regenerating tropical forests," *Int. J. Remote Sens.*, vol. 18, no. 3, pp. 687–694, Feb. 1997.

[73] J. Amini and J. T. S. Sumantyo, "Employing a method on SAR and optical images for forest biomass estimation," *IEEE Trans. Geosci. Remote Sens.*, vol. 47, no. 12, pp. 4020–4026, Dec. 2009.
[74] A. T. Hudak, M. A. Lefsky, W. B. Cohen, and M. Berterretche, "Integration of lidar and Landsat ETM+ data for estimating and mapping forest canopy height," *Remote Sens. Environ.*, vol. 82, no. 2/3, pp. 397–416, Oct. 2002.
[75] C. Wang and J. Qi, "Biophysical estimation in tropical forests using JERS-1 SAR and VNIR imagery. II. Aboveground woody biomass," *Int. J. Remote Sens.*, vol. 29, no. 23, pp. 6827–6849, Dec. 2008.
[76] M. Simard, G. De Grandi, S. Saatchi, and P. Mayaux, "Mapping tropical coastal vegetation using JERS-1 and ERS-1 radar data with a decision tree classifier," *Int. J. Remote Sens.*, vol. 23, no. 7, pp. 1461–1474, Apr. 2002.
[77] M. A. Wulder and D. Seemann, "Forest inventory height update through the integration of lidar data with segmented Landsat imagery," *Can. J. Remote Sens.*, vol. 29, no. 5, pp. 536–543, 2003.
[78] M. Moghaddam, J. L. Dungan, and S. Acker, "Forest variable estimation from fusion of SAR and multispectral optical data," *IEEE Trans. Geosci. Remote Sens.*, vol. 40, no. 10, pp. 2176–2187, Oct. 2002.
[79] P. Muukkonen and J. Heiskanen, "Biomass estimation over a large area based on standwise forest inventory data and ASTER and MODIS satellite data: A possibility to verify carbon inventories," *Remote Sens. Environ.*, vol. 107, no. 4, pp. 617–624, Apr. 2007.
[80] T. Häme, A. Salli, K. Andersson, and A. Lohi, "Forest biomass estimation in Northern Europe using NOAA AVHRR data," *Earth Observ. Q.*, vol. 52, pp. 19–23, 1996.
[81] A. K. Gjertsen, "Two-phase sampling for forest inventory based on satellite imagery," in *Proc. 15th EARSeL Symp.*, 1996, pp. 63–71.
[82] J. Hyyppä, H. Hyyppä, M. Inkinen, M. Engdahl, S. Linko, and Y. Zhu, "Accuracy comparison of various remote sensing data sources in the retrieval of forest stand attributes," *For. Ecol. Manage.*, vol. 128, no. 1, pp. 109–120, Mar. 2000.
[83] Y. Rauste, T. Hame, J. Pulliainen, K. Heiska, and M. Hallikainen, "Radar-based forest biomass estimation," *Int. J. Remote Sens.*, vol. 15, no. 14, pp. 2797–2808, Sep. 1994.
[84] E. Rignot, J. Way, C. Williams, and L. Viereck, "Radar estimates of aboveground biomass in boreal forests of interior Alaska," *IEEE Trans. Geosci. Remote Sens.*, vol. 32, no. 5, pp. 1117–1124, Sep. 1994.
[85] S. A. Sader, R. B. Waide, W. T. Lawrence, and A. T. Joyce, "Tropical forest biomass and successional age class relationships to a vegetation index derived from Landsat TM data," *Remote Sens. Environ.*, vol. 28, pp. 143–156, Apr./Jun. 1989, IN1-IN2, 159-198.
[86] R. F. Nelson, D. S. Kimes, W. A. Salas, and M. Routhier, "Secondary forest age and tropical forest biomass estimation using Thematic Mapper imagery," *Bioscience*, vol. 50, no. 5, pp. 419–431, May 2000.
[87] M. K. Steininger, "Tropical secondary forest regrowth in the Amazon: Age, area and change estimation with Thematic Mapper data," *Int. J. Remote Sens.*, vol. 17, no. 1, pp. 9–27, Jan. 1996.
[88] M. A. Spanner, L. L. Pierce, D. L. Peterson, and S. W. Running, "Remote sensing of temperate coniferous forest leaf area index. The influence of canopy closure, understory vegetation and background reflectance," *Int. J. Remote Sens.*, vol. 11, no. 1, pp. 95–111, Jan. 1990.
[89] D. Lu and M. Batistella, "Exploring TM image texture and its relationships with biomass estimation in Rondônia, Brazilian Amazon," *Acta Amazonica*, vol. 35, no. 2, pp. 261–268, Apr.–Jun. 2005.
[90] C. J. Tucker, "Red and photographic infrared linear combinations for monitoring vegetation," *Remote Sens. Environ.*, vol. 8, no. 2, pp. 127–150, May 1979.
[91] A. Huete, C. Justice, and H. Liu, "Development of vegetation and soil indices for MODIS-EOS," *Remote Sens. Environ.*, vol. 49, no. 3, pp. 224–234, Sep. 1994.
[92] A. R. Huete, R. D. Jackson, and D. F. Post, "Spectral response of a plant canopy with different soil backgrounds," *Remote Sens. Environ.*, vol. 17, no. 1, pp. 37–53, Feb. 1985.
[93] C. Leprieur, M. M. Verstraete, B. Pinty, and A. Chehbouni, "NOAA/AVHRR vegetation indices: Suitability for monitoring fractional vegetation cover of the terrestrial biosphere," in *Proc. 6th ISPRS Int. Symp. Phys. Meas. Signatures Remote Sens.*, 1994, pp. 1103–1110.
[94] A. Karnieli, Y. J. Kaufman, L. Remer, and A. Wald, "AFRI—Aerosol free vegetation index," *Remote Sens. Environ.*, vol. 77, no. 1, pp. 10–21, Jul. 2001.
[95] M. Zoran and S. Stefan, "Climatic changes effects on spectral vegetation indices for forested area analysis from satellite data," in *Proc. 2nd Environ. Phys. Conf.*, 2006, pp. 73–83.
[96] J. Ardö, "Volume quantification of coniferous forest compartments using spectral radiance recorded by Landsat Thematic Mapper," *Int. J. Remote Sens.*, vol. 13, no. 9, pp. 1779–1786, Jun. 1992.
[97] C. M. Trotter, J. R. Dymond, and C. J. Goulding, "Estimation of timber volume in a coniferous plantation forest using Landsat TM," *Int. J. Remote Sens.*, vol. 18, no. 10, pp. 2209–2223, Jul. 1997.
[98] D. Lu, P. Mausel, E. Brondizio, and E. Moram, "Above-ground biomass estimation of successional and mature forests using TM images in the Amazon Basin,"in *Proc. Symp. Geospatial Theory, Process. Appl.*, 2002. [Online]. Available: http://www.isprs.org/proceedings/XXXIV/part4/pdfpapers/059.pdf
[99] R. M. Haralick, K. Shanmugam, and I. Dinstein, "Textural features for image classification," *IEEE Trans. Syst., Man, Cybern.*, vol. SMC-3, no. 6, pp. 610–621, Nov. 1973.
[100] D. He and L. Wang, "Texture unit, texture spectrum, and texture analysis," *IEEE Trans. Geosci. Remote Sens.*, vol. 28, no. 4, pp. 509–512, Jul. 1990.
[101] M. Unser, "Texture classification and segmentation using wavelet frames," *IEEE Trans. Image Process.*, vol. 4, no. 11, pp. 1549–1560, Nov. 1995.
[102] R. Riou and F. Seyler, "Textural analysis of tropical rain forest infrared satellite images," *Photogramm. Eng. Remote Sens.*, vol. 63, pp. 515–521, May 1997.
[103] R. Connors and C. Harlow, "A theoretical comparison of texture algorithms," *IEEE Trans. Pattern Anal. Mach. Intell.*, vol. PAMI-2, no. 3, pp. 204–222, May 1980.
[104] S. E. Franklin and D. R. Peddle, "Spectral texture for improved class discrimination in complex terrain," *Int. J. Remote Sens.*, vol. 10, no. 8, pp. 1437–1443, Aug. 1989.
[105] D. J. Marceau, P. J. Howarth, J. M. Dubois, and D. J. Gratton, "Evaluation of grey level co-occurrence matrix method for land-cover classification using SPOT imagery," *IEEE Trans. Geosci. Remote Sens.*, vol. 28, no. 4, pp. 513–519, Jul. 1990.
[106] D. He and L. Wang, "Unsupervised textural classification of images using the texture spectrum," *Pattern Recognit.*, vol. 25, no. 3, pp. 247–255, Mar. 1992.
[107] M. Augusteijn, L. E. Clemens, and K. A. Shaw, "Performance evaluation of texture measures for ground cover identification in satellite images by means of a neural network classifier," *IEEE Trans. Geosci. Remote Sens.*, vol. 33, no. 3, pp. 616–626, May 1995.
[108] R. M. Lark, "Geostatistical description of texture on an aerial photograph for discriminating classes of land cover," *Int. J. Remote Sens.*, vol. 17, no. 11, pp. 2115–2133, Jul. 1996.
[109] S. Ryherd and C. Woodcock, "Combining spectral and texture data in the segmentation of remotely sensed images," *Photogramm. Eng. Remote Sens.*, vol. 62, pp. 181–194, 1996.
[110] S. E. Franklin, R. J. Hall, L. M. Moskal, A. J. Maudie, and M. B. Lavigne, "Incorporating texture into classification of forest species composition from airborne multispectral images," *Int. J. Remote Sens.*, vol. 21, no. 1, pp. 61–79, Jan. 2000.
[111] A. N. Nyoungui, E. Tonye, and A. Akono, "Evaluation of speckle filtering and texture analysis methods for land cover classification from SAR images," *Int. J. Remote Sens.*, vol. 23, no. 9, pp. 1895–1925, May 2002.
[112] E. Podest and S. Saatchi, "Application of multiscale texture in classifying JERS-1 radar data over tropical vegetation," *Int. J. Remote Sens.*, vol. 23, no. 7, pp. 1487–1506, Apr. 2002.
[113] R. J. Dekker, "Texture analysis and classification of ERS SAR images for map updating of urban areas in The Netherlands," *IEEE Trans. Geosci. Remote Sens.*, vol. 41, no. 9, pp. 1950–1958, Sep. 2003.
[114] M. L. R. Sarker, Y. Ban, and J. Nichol, "Comparison of pixel-based, object-based and sequential masking classification procedures for land use and land cover mapping using multiple sensor SAR in Sweden," *Asian J. Geoinf.*, vol. 8, no. 1, pp. 25–30, Jan. 2008.
[115] W. B. Cohen and T. A. Spies, "Estimating structural attributes of Douglas-fir/Western Hemlock forest stands from Landsat and SPOT imagery," *Remote Sens. Environ.*, vol. 41, no. 1, pp. 1–17, Jul. 1992.
[116] B. A. St-Onge and F. Cavayas, "Estimating forest stand structure from high resolution imagery using the directional variogram," *Int. J. Remote Sens.*, vol. 16, no. 11, pp. 1999–2021, Jul. 1995.
[117] B. A. St-Onge and F. Cavayas, "Automated forest structure mapping from high resolution imagery based on directional

semivariogram estimates," *Remote Sens. Environ.*, vol. 61, no. 1, pp. 82–95, Jul. 1997.
[118] M. A. Wulder, S. E. Franklin, and M. B. Lavigne, "High spatial resolution optical image texture for improved estimation of forest stand leaf area index," *Can. J. Remote Sens.*, vol. 22, pp. 441–449, 1996.
[119] S. E. Franklin, *Remote Sensing for Sustainable Forest Management*. Boca Raton, Florida: CRC Press, 2001.
[120] T. M. Kuplich and P. J. Curran, "Estimating texture independently of tone in simulated images of forest canopies," in *Proc. Brazilian Symp. Remote Sens.*, 2003, pp. 2209–2216.
[121] G. J. Hay, K. O. Niemann, and G. F. McLean, "An object-specific image-texture analysis of H-resolution forest imagery," *Remote Sens. Environ.*, vol. 55, no. 2, pp. 108–122, Feb. 1996.
[122] C. S. A. Wallace, J. M. Watts, and S. R. Yool, "Characterizing the spatial structure of vegetation communities in the Mojave Desert using geostatistical techniques," *Comput. Geosci.*, vol. 26, no. 4, pp. 397–410, May 2000.
[123] S. E. Franklin, M. A. Wulder, and G. R. Gerylo, "Texture analysis of IKONOS panchromatic data for Douglas-fir forest age class separability in British Columbia," *Int. J. Remote Sens.*, vol. 22, no. 13, pp. 2627–2632, Sep. 2001.
[124] A. Puissant, J. Hirsch, and C. Weber, "The utility of texture analysis to improve per-pixel classification for high to very high spatial resolution imagery," *Int. J. Remote Sens.*, vol. 26, no. 4, pp. 733–745, Feb. 2005.
[125] S. Tuominen and A. Pekkarinen, "Performance of different spectral and textural aerial photograph features in multi-source forest inventory," *Remote Sens. Environ.*, vol. 94, no. 2, pp. 256–268, Jan. 2005.
[126] S. E. Franklin, M. A. Wulder, and M. B. Lavigne, "Automated derivation of geographic window sizes for use in remote sensing digital image texture analysis," *Comput. Geosci.*, vol. 22, no. 6, pp. 665–673, Jul. 1996.
[127] D. Chen, D. A. Stow, and P. Gong, "Examining the effect of spatial resolution and texture window size on classification accuracy: An urban environment case," *Int. J. Remote Sens.*, vol. 25, no. 11, pp. 2177–2192, Jun. 2004.
[128] J. P. M. Overman, H. J. L. Witte, and J. G. Saldarriaga, "Evaluation of regression models for above-ground biomass determination in Amazon rainforest," *J. Trop. Ecol.*, vol. 10, pp. 207–218, 1994.
[129] S. Brown, *Estimating Biomass and Biomass Change of Tropical Forests: A Primer*. United Nations, Rome: FAO, 1997.
[130] C. E. Woodcock and A. H. Strahler, "The factor of scale in remote sensing," *Remote Sens. Environ.*, vol. 21, no. 3, pp. 311–332, Apr. 1987.
[131] R. M. Haralick, "Statistical and structural approaches to texture," *Proc. IEEE*, vol. 67, no. 5, pp. 786–804, May 1979.
[132] F. T. Ulaby, F. Kouyate, B. Brisco, and T. H. L. Williams, "Textural information in SAR images," *IEEE Trans. Geosci. Remote Sens.*, vol. GRS-24, no. 2, pp. 235–245, Mar. 1986.
[133] F. Dell'Acqua and P. Gamba, "Discriminating urban environments using multiscale texture and multiple SAR images," *Int. J. Remote Sens.*, vol. 27, no. 18, pp. 3797–3812, Sep. 2006.
[134] M. Unser, "Sum and difference histograms for texture classification," *IEEE Trans. Pattern Anal. Mach. Intell.*, vol. PAMI-8, no. 1, pp. 118–125, Jan. 1986.
[135] A Wijaya and R. Gloaguen, "Fusion of ALOS Palsar and Landsat ETM data for land cover classification and biomass modeling using non-linear methods," in *Proc. IGARSS*, 2009, vol. 3, pp. 581–584.
[136] L. Coulibaly, P. Migolet, G. H. Adegbidi, R. Fournier, and E. Hervet, "Mapping aboveground forest biomass from IKONOS satellite image and multi-source geospatial data using neural networks and a kriging interpolation," in *Proc. IGARSS*, 2008, vol. 3, pp. 298–301.
[137] A. C. Almeida, P. L. C. Barros, J. H. A. Monteiro, and B. R. P. Rocha, "Estimation of aboveground forest biomass in Amazonia with neural networks and remote sensing," *IEEE Latin Amer. Trans.*, vol. 7, no. 1, pp. 27–32, Mar. 2009.
[138] P. A. Townsend, "Estimating forest structure in wetlands using multitemporal SAR," *Remote Sens. Environ.*, vol. 79, no. 2/3, pp. 288–304, Feb. 2002.
[139] H. Franco-Lopez, A. R. Eck, and M. E. Bauer, "Estimation and mapping of forest density, volume and cover type using the k-nearest neighbours method," *Remote Sens. Environ.*, vol. 77, no. 3, pp. 251–274, Sep. 2001.
[140] D. A. Belsley, *Conditioning Diagnostics*. New York: Wiley, 1991.
[141] M. H. Kutner, C. J. Nachtsheim, J. Neter, and W. Li, *Applied Linear Statistical Models*. Boston, MA: McGraw-Hill, 2005.
[142] C. M. Douglas, E. A. Peck, and G. G. Vining, *Introduction to Linear Regression Analysis*. Hoboken, NJ: Wiley, 2006.
[143] D. A. Belsley, E. Kuh, and R. E. Welsch, *Regression Diagnostics: Identifying Influential Data and Sources of Collinearity*. New York: Wiley, 1980.
[144] K. L. Castro, G. A. Sanchez-Azofeifa, and B. Rivard, "Monitoring secondary tropical forests using space-borne data: Implications for Central America," *Int. J. Remote Sens.*, vol. 24, no. 9, pp. 1853–1894, May 2003.
[145] P. M. Mather, *Computer Processing of Remotely Sensed Images: An Introduction*. New York: Wiley, 1999.
[146] R. A. Schowengerdt, *Techniques for Image Processing and Classification in Remote Sensing*. New York: Academic, 1983.
[147] P. J. Curran, "Estimating green LAI from multispectral aerial photography," *Photogramm. Eng. Remote Sens.*, vol. 49, pp. 1709–1720, 1983.
[148] C. D. Elvidge and C. Zhikang, "Comparison of broad-band and narrow-band red and near-infared vegetation indices," *Remote Sens. Environ.*, vol. 54, no. 1, pp. 38–48, Oct. 1995.
[149] G. A. Blackburn and C. M. Steele, "Towards the remote sensing of matorral vegetation physiology: Relationships between spectral reflectance, pigment, and biophysical characteristics of semiarid bush-land canopies," *Remote Sens. Environ.*, vol. 70, no. 3, pp. 278–292, Dec. 1999.
[150] X. Gao, A. R. Huete, W. Ni, and T. Miura, "Optical–biophysical relationships of vegetation spectra without background contamination," *Remote Sens. Environ.*, vol. 74, no. 3, pp. 609–620, Dec. 2000.
[151] P. J. Gibson and C. H. Power, *Introductory Remote Sensing: Digital Image Processing and Applications*. London, U.K.: Routledge, 2000.
[152] E. Boegh, H. Soegaard, N. Broge, C. B. Hasager, N. O. Jensen, K. Schelde, and A. Thomsen, "Airborne multispectral data for quantifying leaf area index, nitrogen concentration, and photosynthetic efficiency in agriculture," *Remote Sens. Environ.*, vol. 81, no. 2, pp. 179–193, Aug. 2002.
[153] J. R. Jensen, *Remote Sensing of the Environment: An Earth Resource Perspective*. Upper Saddle River, NJ: Prentice-Hall, 2007.
[154] E. F. Moran, E. Brondizio, P. Mausel, and Y. Wu, "Integrating Amazonian vegetation, land-use, and satellite data: Attention to differential patterns and rates of secondary succession can inform future policies," *BioScience*, vol. 22, pp. 323–341, 1994.
[155] D. L. Peterson, M. A. Spanner, S. W. Running, and K. B. Teuber, "Relationship of Thematic Mapper simulator data to leaf area index of temperate coniferous forests," *Remote Sens. Environ.*, vol. 22, no. 3, pp. 323–341, Aug. 1987.
[156] S. R. Herwitz, D. L. Pctersou, and J. K. Eastman, "Thematic Mapper detection of changes in the leaf area of closed canopy pine plantations in Central Massachusetts," *Remote Sens. Environ.*, vol. 30, no. 2, pp. 129–140, Nov. 1990.
[157] K. S. Fassnacht, S. T. Gower, M. D. MacKenzie, E. V. Nordheim, and T. M. Lillesand, "Estimating the leaf area index of North Central Wisconsin forests using the Landsat Thematic Mapper," *Remote Sens. Environ.*, vol. 61, no. 2, pp. 229–245, Aug. 1997.
[158] R. B. Myneni, J. Dong, C. J. Tucker, R. K. Kaufmann, P. E. Kauppi, J. Liski, L. Zhou, V. Alexeyev, and M. K. Hughes, "A large carbon sink in the woody biomass of northern forests," *Proc. Nat. Acad. Sci. U.S.A.*, vol. 98, no. 26, pp. 14 784–14 789, Dec. 2001.
[159] W. J. Ripple, "Asymptotic reflectance characteristics of grass vegetation," *Photogramm. Eng. Remote Sens.*, vol. 51, pp. 1915–1921, 1985.
[160] N. C. Coops and D. Culvenor, "Utilizing local variance of simulated high spatial resolution imagery to predict spatial pattern of forest stands," *Remote Sens. Environ.*, vol. 71, no. 3, pp. 248–260, Mar. 2000.
[161] W. A. Salas, M. J. Ducey, E. Rignot, and D. Skole, "Assessment of JERS-1 SAR for monitoring secondary vegetation in Amazonia: I. Spatial and temporal variability in backscatter across a chrono-sequence of secondary vegetation stands in Rondonia," *Int. J. Remote Sens.*, vol. 23, no. 7, pp. 1357–1379, Apr. 2002.
[162] E. S. Kasischke, J. M. Melack, and M. C. Dobson, "The use of imaging radars for ecological applications—A review," *Remote Sens. Environ.*, vol. 59, no. 2, pp. 141–156, Feb. 1997.
[163] J. T. Pulliainen, P. J. Mikkela, M. T. Hallikainen, and J. Ikonen, "Seasonal dynamics of C-band backscatter of boreal forests with applications to biomass and soil moisture estimation," *IEEE Trans. Geosci. Remote Sens.*, vol. 34, no. 3, pp. 758–770, May 1996.
[164] J. Shi and J. Dozier, "Mapping seasonal snow with SIR-C/X-SAR in mountainous areas," *Remote Sens. Environ.*, vol. 59, no. 2, pp. 294–307, Feb. 1997.

Janet E. Nichol received the B.Sc. degree from the University of London, London, U.K., the M.A. degree from the University of Colorado, Boulder, and the Ph.D. degree from the University of Aston, Birmingham, U.K.

She subsequently worked in the U.K., Nigeria, Singapore, and the Republic of Ireland as a University Lecturer. Since 2001, she has been teaching and undertaking research in the Department of Land Surveying and Geo-Informatics, The Hong Kong Polytechnic University, Kowloon, Hong Kong. She has a background in physical geography, specializing in remote sensing and ecology. Her research interests are in the application of remote sensing techniques to environmental assessment and monitoring, including urban heat island, vegetation mapping, air quality monitoring, quaternary climate change, and aspects of image processing. She has published widely on these topics and is a reviewer for journals specializing in remote sensing, planning, and environmental issues.

Md. Latifur Rahman Sarker was born in Gaibandha, Bangladesh, in 1968. He received the M.S. degree in geodesy and geoinformatics from the Royal Institute of Technology (KTH), Stockholm, Sweden, in 2005 and the Ph.D. degree in biomass estimation using remote sensing techniques from The Hong Kong Polytechnic University, Kowloon, Hong Kong, in 2010.

He is currently working as a Research Associate with the Department of Land Surveying and Geo-Informatics, The Hong Kong Polytechnic University. He is also with the Department of Geography and Environmental Studies, Rajshahi University, Rajshahi, Bangladesh. His research experience includes the application of optical and synthetic aperture radar (SAR) data for land use/land cover mapping and biomass estimation, wavelet image fusion of SAR and optical data, texture processing, artificial neural network, and feature extraction.